Rake Angle Effects on Ultrasonic-Assisted Edge Trimming of Multidirectional CFRP Laminates

Mohamed Helmy (mohamed.osama@bhit.bu.edu.eg)
Benha University
Hassan El-Hofy
University for Science and Technology (E-JUST)
Hiroyuki Sasahara
Tokyo University of Agriculture and Technology
Mohamed El-Hofy
University for Science and Technology (E-JUST)

Research Article

Keywords: Edge trimming, multidirectional, CFRP, Ultrasonic, Rake angle

Posted Date: March 1st, 2021

DOI: https://doi.org/10.21203/rs.3.rs-239155/v1

Rake angle effects on ultrasonic-assisted edge trimming of multidirectional CFRP laminates

Mohamed O. Helmy[1, *], Hassan El-Hofy[2,3], Hiroyuki Sasahara[4], M. H. El-Hofy[2,5]

[1] Department of Mechanical Engineering, Benha Faculty of Engineering, Benha University, 13518, Egypt
[2] Industrial and Manufacturing Engineering Department, School of Innovative Design Engineering, Egypt-Japan University for Science and Technology (E-JUST), Alexandria 21934, Egypt
[3] Faculty of Engineering, Alexandria University, Alexandria, 21544, Egypt
[4] Department of Mechanical Systems Engineering, Tokyo University of Agriculture and Technology, 2-24-16 Naka-cho, Koganei, Tokyo, 184-8588, Japan
[5]Advanced Manufacturing Research Centre with Boeing, The Universality of Sheffield, Advanced Manufacturing Park, Wallis way, Rotherham, S60 5TZ, UK

*Corresponding author: Mohamed.osama@bhit.bu.edu.eg

Abstract

Machining of CFRP composites is a process frequently accompanied with adverse effects on machined surface. The geometry of the cutting tool, linked primarily to influencing the cutting mechanism, could largely influence the induced damage. An optimum combination of tool material and geometry could improve the cut quality and prolong the tool life. This article investigates the effect of using tools having different rake angles in an ultrasonic-assisted edge trimming operation when cutting multidirectional CFRP laminates. A full-factorial experimental design was adopted to analyse the effect of parameters typically cutting speed, feed rate, rake angle, amplitude, and their interactions on machining performance indicators captured which were the cutting forces, tool wear, chip temperature, and surface roughness. The results showed that UAM mode contributed to the increase in cutting forces, tool wear, and chip temperature compared to conventional mode. On the other hand, UAM mode improved the quality of the machined surface. Additionally, the ultrasonic mode enhances the material removal mechanism using a tool with a negative rake angle.

Keywords: Edge trimming, multidirectional, CFRP, Ultrasonic, Rake angle

1. Introduction

Lightweighting is one of the main drivers behind the growing demand for carbon fiber reinforced plastics (CFRP) composites. This composite material is a good candidate for many applications such as automotive, spacecraft, and sports equipment. It lends itself to the aerospace industry for good qualities such as the higher strength-to-weight ratio, which reflects on performance and fuel consumption downstream. Being made to near-net-shape necessitates a subsequent edge trimming operation to meet the industrial standards with respect to dimension and quality [1, 2]. Trimming is feasible by either conventional ways such as milling or nonconventional methods such as abrasive water jet machining [3, 4]. However, cutting by conventional need to overcome the challenging heterogeneity and anisotropy of the CFRP laminates and the machining induced damage [5]. This is

found in many forms/locations either at free edges such as fibre pull-out and delamination or in form of on/sub-surface such as fibre pull-out and matrix smearing or degradation [6]. Defects and their costly scrap toll were the motive to study the factors affecting these damages in order to eliminate/mitigate for the first-time-right or zero-defect production concepts. In this context, it was reported that increasing cutting speeds with a lower feed rates provides better surface quality [7, 8]. However, this will be at the expense of increased friction between the cutting tool and workpiece, which reduces tool life. Fundamentally, for a unidirectional CFRP laminate, the defects generated from cutting are mainly influenced by the cutting direction corresponding to the fiber orientations (fibre cutting angle) [9, 10].

The tool geometry/angles dictate the engagement between the cutting tool and the workpiece and, thereby, multiple scenarios of material removal/separation and, subsequently, the occurrence of different shapes of chips [11]. Therefore, sharp cutting edges are required for precise fracturing of the carbon fibers, which in turn reduces the damages [12]. Other factors contributing to the chip formation include edge rounding caused by tool coating or high abrasive wear. The latter is due to the abrasive nature of the carbon fibers [13] which will eventually lead to unwanted deterioration in the form of delamination and/or subsurface damage [14]. Add to this complexity, the machining process of CFRP is sensitive to direction in a way that quality aspects in longitudinal (roughness of plies measured parallel to edge) was found dependant on tool geometry as well as the cutting conditions which was not the case in transverse roughness (i.e. measured perpendicular) which was dependant on only on tool geometry [15]. Therefore, the machining parameters and cutting tool specifications should be selected carefully for cutting of CFRP laminates.

For tools with defined cutting edge geometry, Polycrystalline diamond (PCD) and carbide cutters have been widely used for cutting composite materials. Studies on the effect of tool angles revealed that the relief angle has no significant effect on the chip formation mechanism. On the other side, a larger rake angle enhances the machined surface quality and reduces subsurface defects [16]. Alternative abrasive tool solutions with an undefined geometry or angles can be used for cutting CFRP. Diamond abrasive cutters, for instance, with all the inherent good qualities of diamond such as low thermal expansion coefficient, high hardness, and high thermal conductivity [8, 11] may suffer from deficient chip evacuation which introduces thermal damages to the machined surfaces due to rubbing [17, 18].

The influence of cutting tool geometry and fibre orientation was investigated by many. Both rake angle and fiber orientation were said to determine the chip formation mechanism [10, 19]. When cutting fibers oriented at 0° and 135° using a positive rake angle tool, the fibers are fractured due to bending. On the other hand, when using a negative rake angle tool, the chips are formed as a result of buckling of fibers. The variation in chip formation may affect the extent of subsurface defects [20]. These defects are dependent on the depth of cut as well as tool geometry features especially the rake angle. It is found that cutting fibers in the orientations between 120° and 150° with a depth of cut within the range of 100 μm, subsurface damage is inevitable [10]. Jahromi et al. also confirmed that the fiber cutting angle and tool rake angle were the

main factors affecting the chip formation mechanism [21]. During the orthogonal cutting of unidirectional fiber composite, it was revealed that the chips would slide on the rake face when the cutting angle is more than (90^o + rake angle) while being pushed when the cutting angle is less than (90^o + rake angle) [22]. Moreover, they reported other features such as nose radius to have no effect on chip formation mechanism when the cutting angle is greater than (90^o + rake angle). Mkaddem et al. [23] found that cutting forces decreases dramatically with increasing rake angles owing to the reduction of the contact area between the rake face and workpieces, which increasing the chip length. However, the cutting force increased when the rake angle exceeded 20^o. Generally, increasing the rake angle improves chip disposal and enhances the machined surface quality. Recently, Sheikh-Ahmad et al used tools with different rake angles in a slotting test to study cutting forces [24]. They also used a cutting tribosystem to estimate the coefficient of friction for different fibre orientations. The setup used eliminate the need to closed tribosystem mostly reliant on moving balls or pins which assume idealised contact conditions that lacks the shearing, bending and spring-back associated with real cutting. Coefficient of friction increased with increase in rake angle from -15 to 15 and it was dependent on fibre cutting angle with the peak coefficient of friction occurring at 115^o fibre cutting angle [25].

The concept of introducing minute oscillation (microns) at ultrasonic frequency to the process kinematics makes the so-called ultrasonic-assisted machining (UAM) which is proving its potential nowadays in cutting the hard-to-cut materials such as ceramics and composites [26]. This facilitates/enhances the chip breakage and increases the possibility for machining difficult material at a relatively lower cost [27]. Ultrasonic assisted drilling of CFRP, for example, contributed to lowering the average thrust force by a margin of 30% [28]. However, the intermittent cutting action adds more friction load on the cutting tool, which increases the tool wear rate and, eventually, the cutting temperature [28, 29].

From the aforementioned literature, only limited investigations into the effect of cutting-edge geometries on machining of CFRP in conventional machining of CFRP were found let alone the state-of-the-art ultrasonic-assisted cutting. Therefore, this article presents an investigation into the effect of different rake angles used in the ultrasonic-assisted edge trimming process of multidirectional CFRP laminates. The process variable parameters were the cutting speed, feed rate, rake angle, and amplitude. While the performance characteristics captured in the scope of this study were the cutting forces, tool wear, cutting temperature (chip temperature), and surface roughness. Statistical analysis was conducted to address the effect of these parameters and their interactions on machining responses.

2. Experimental setup and procedures

2.1 Material preparation

The multidirectional CFRP laminates used in this investigation were autoclave cured stack of unidirectional (UD) prepregs containing intermediate modulus (294 GPa) carbon fibers impregnated within an epoxy resin matrix. The prepregs were manufactured by Toray Industries with material properties listed in Table 1. Prepreg plies were manually laid up, vacuum bagged in a clean room, and subsequently cured

using autoclave for consolidation. The typical cure cycle included ramping temperature up to a cure temperature of 180ºC ± 5ºC for 120 min under 7 bar pressure assuming the same degree of cure and glass temperature for all samples having identical cure cycles. All cured panels passed the subsequent check for voids/defects using a gantry ultrasonic C-scan machine.

Table 1: CFRP laminate properties

CFRP characteristics	Value
Weave type	UD (non-woven)
Fibre areal weight	268 (g/m^2)
Fiber volume fraction	60%
Fiber orientation angle	[45˚/0˚/135˚/90˚]5$_S$
Number of plies	40 plies
Ply thickness	0.26 mm
Resin type	3911
Carbon fiber type	T800SC
Number of filaments per roving	24K
Manufacturing method	Hand-layup, autoclave cure

2.2 Experimental setup

Edge trimming experiments were conducted on a Mazak FJV-250 UHS 5-axis CNC milling machine. The machine has a maximum spindle speed of 25,000 rpm and a 22kW spindle motor power. The experiments were conducted using an uncoated single straight flute carbide end mill with three different rake angles (-15º, 0º and 15º) from OSG Co., Japan, as shown in figure 1. Table 2 lists the specifications of the end mill.

The design is identical to those used previously by Sheikh-Ahmad et al [25] except in cutting length which was 35 mm instead of 30 mm for maximum tool utilization reasons in order to accommodate three specimens having 10.4 mm thickness. Therefore, a collet with adjustable length was utilized to set the cutting distance between the tool shank and the top surface of CFRP constant for each experimental test.

An ultrasonic vibration table, type UST-150-20K, was attached to the CNC machine table to generate the oscillation movement in the vertical direction (Z-axis). The table is capable of generating oscillations with frequency in the range of 20 kHz ± 1.5 kHz. Ultrasonic amplitude can be tuned to up to 6 µm. To measure oscillation amplitude there are different methods such as laser vibrometer, high-speed camera, gap sensor, or using a teardrop accelerometer. However, a gap sensor PU-02A with a resolution of 0.3µm was utilized in the current investigation.

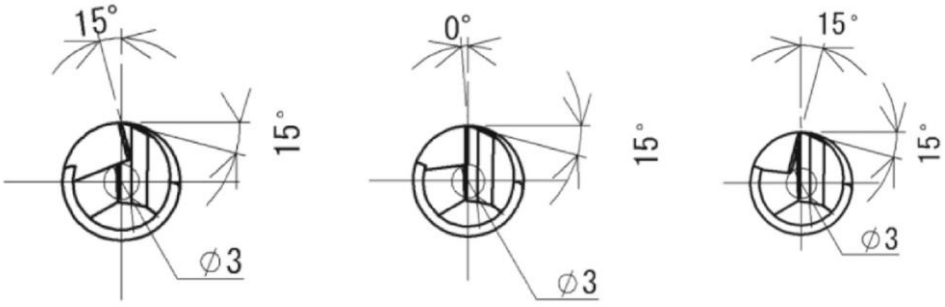

Figure 1: Three different rake angles (15º, 0º, and -15º) for single flute end mill

Table 2: Specifications of OSG end mill

Diameter	10 mm	**Helix angle**	0 deg (straight flute)
Number of flutes	One flute (cutting edge)	**Primary relief**	15 deg
Cutting length	35 mm	**Coating**	Bright finish (non-coated)
End mill length	100 mm	**Rake angle**	-15, 0, 15 deg

CFRP coupons were sectioned into smaller specimens having dimensions of 80×40×10.4 mm (WxLxT) using a high-speed precision cutting machine FINE CUT model HS-45A C. A special aluminium fixture was designed and fabricated for holding the CFRP coupons in a pocket with a dimension of 80mm × 35mm × 10.4mm. Figure 2 shows the full experimental setup used in the ultrasonic-assisted edge trimming of multidirectional CFRP trials.

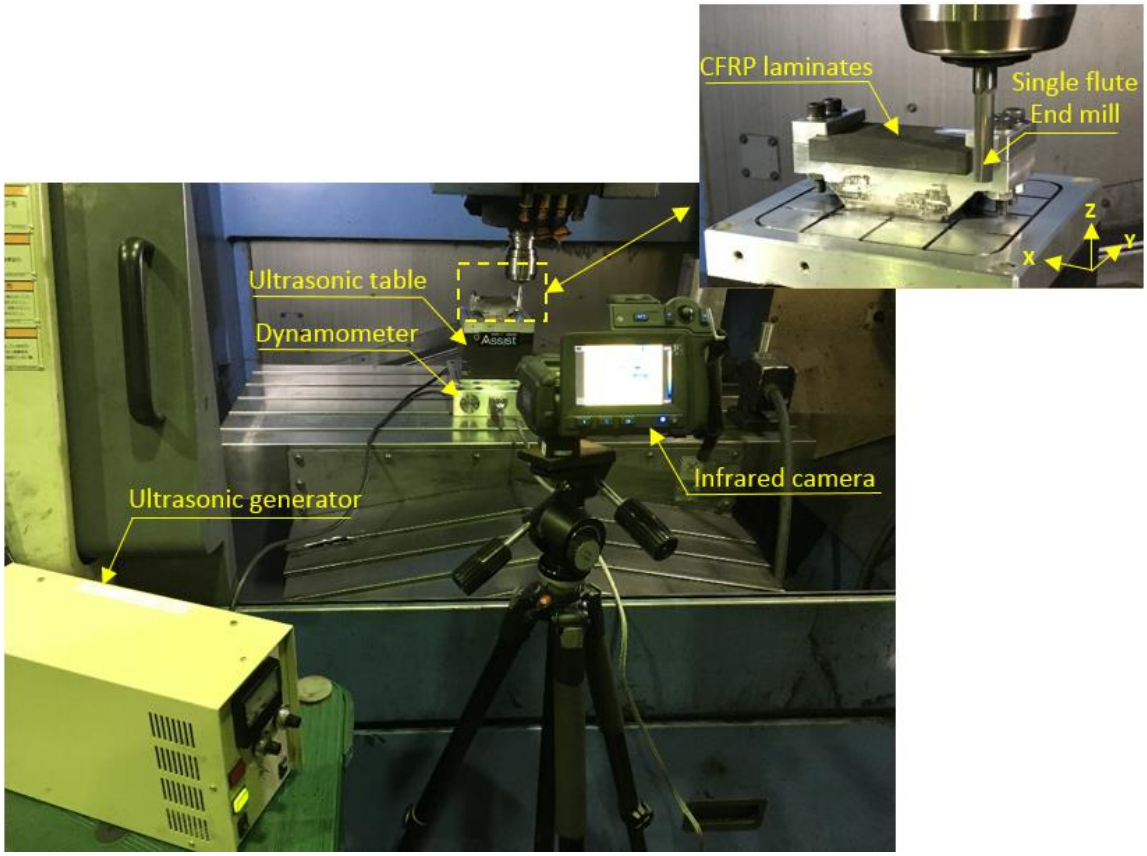

Figure 2: Experimental setup for ultrasonic-assisted edge trimming of CFRP using a defined tool geometry

A full factorial design-of-experiment was employed to investigate the effect of the four parameters and their interactions on the machining responses, i.e., cutting forces, chip temperature, tool wear, and surface integrity of CFRP, at a 95% confidence level. Table 3 lists the factors and their levels, which were selected based on the pilot experiment. Only amplitude was selected to be equal to 1/2 fiber diameter (2.25μ) and full fiber diameter (4.5μ). On the other side, zero amplitude represented the conventional cutting mode. The 54 experiments in total were conducted using a

set of 16 end mills where a fresh cutting edge from the end mill was used in each experiment. All experiments were conducted removing a fixed depth of cut of 500 µm while adopting the down milling mode in the dry cutting environment.

Table 3: Process parameters and their levels

Parameters	Symbol	Units	Levels		
Spindle speed	A	Rpm	5000		10000
Feed rate	B	mm/min	25	50	100
Rake angle	C	Degree	-15	0	15
Amplitude	D	µm	0	2.25	4.5

A Kistler's Type 9139AA platform dynamometer was used for capturing feed force (Fx) and normal force (Fy) at a sampling rate of 5000 Hz. The thrust force (Fz) was neglected in this study since the cutting length of the tool is larger than the laminate thickness, and the tool does not possess helix, which means less contribution to the edge trimming process. Specimens were air dusted following machining using compressed air in the vicinity of the machine wearing adequate personal protective equipment. A digital measuring microscope (KEYENCE-VHX-6000) was used for measuring tool wear and surface integrity. A high-resolution infrared camera FLIR T650sc was used for mounting the chip temperature. Surface roughness in terms of arithmetical mean height (Ra) was measured in the transverse direction using a 3D laser microscope KEYENCE model VK-X100. Ra was measured at tool engagement (10 mm) and tool disengagement (70 mm) in order to correlate the surface quality with the tool condition as shown in figure 3.

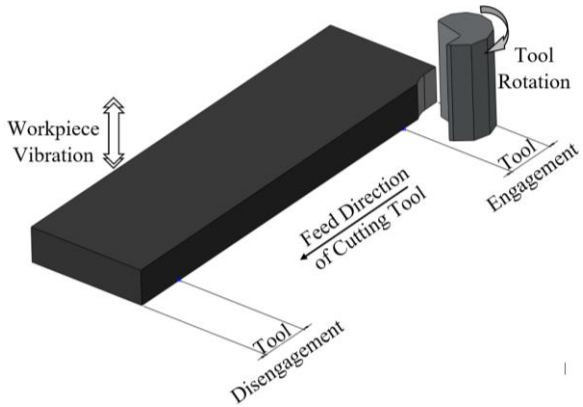

Figure 3: Schematic of ultrasonic-assisted edge trimming of CFRP laminates

The variation of average flank wear (VB) was measured along the entire cutting thickness (10.4 mm) was then averaged to represent the tool wear across all CFRP plies.

3. Results and discussions

3.1 Cutting forces

Cutting forces are considered of the primary response that reflects the efficiency of cutting operations. Force components captured were in the feed direction (Fx), which is tangential and radial direction (Fy). The use of maximum cutting force component Fx was preferred over the average values of Fx, especially when using a single flute end mill to give a better representation of forces. This component was recorded when the tool has fully engaged with the CFRP workpiece. The recorded cutting force was relatively high than expected for such small depth of cut (0.5 mm) used as it combines the force from cutting as well as dynamic forces from the vibrating setup.

Figure 4 shows a Pareto chart for the standardized effects of Fx. It's clearly observed that spindle speed (A) is the most significant factor, followed by the rake angle (C) and the magnitude of vibration amplitude (D), and the interaction (AC). The higher the cutting speed, the smaller is the

chip thickness, which in turn reduces the feed force.

Rake angles are considered the second main significant factor is owing to their primary contribution to the chip formation mechanism either by fiber buckling, delamination, continuous/discontinuous fiber cutting, or macro-fracture [6]. A positive rake angle (+15°) reduces the feed force Fx dramatically compared to 0° and -15°, as shown in Figure 5. The interpretation of this phenomenon is related to the cutting mechanism of each angle. In the case of a positive rake angle (+15°), the fracture of fibers mainly occurs by tension and shear, which trim the carbon fibers easily. Favorable cutting mode with lower forces was also attributed to the +15° rake angle tool despite the higher coefficient of friction reported in cutting unidirectional laminates [25].

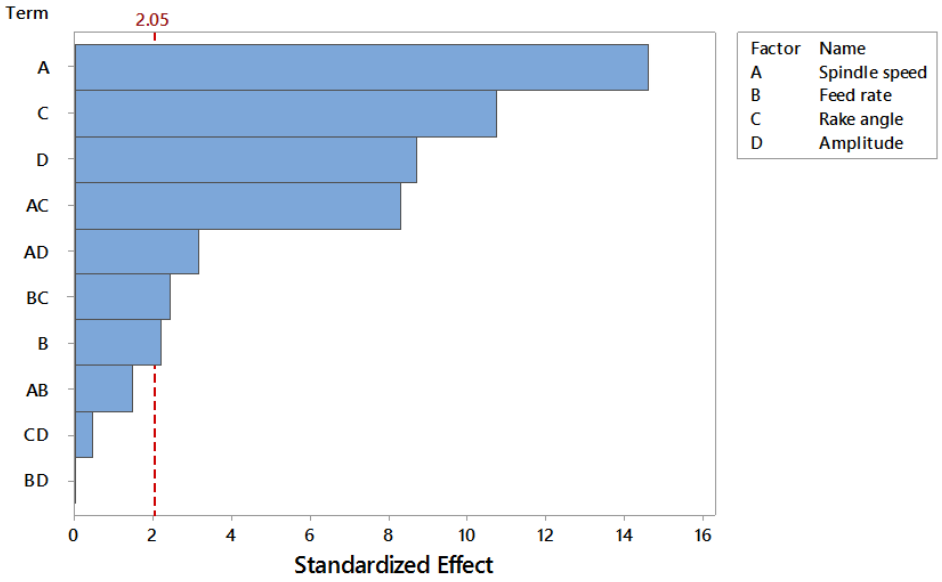

Figure 4: Pareto chart of the standardized effects Fx-Max

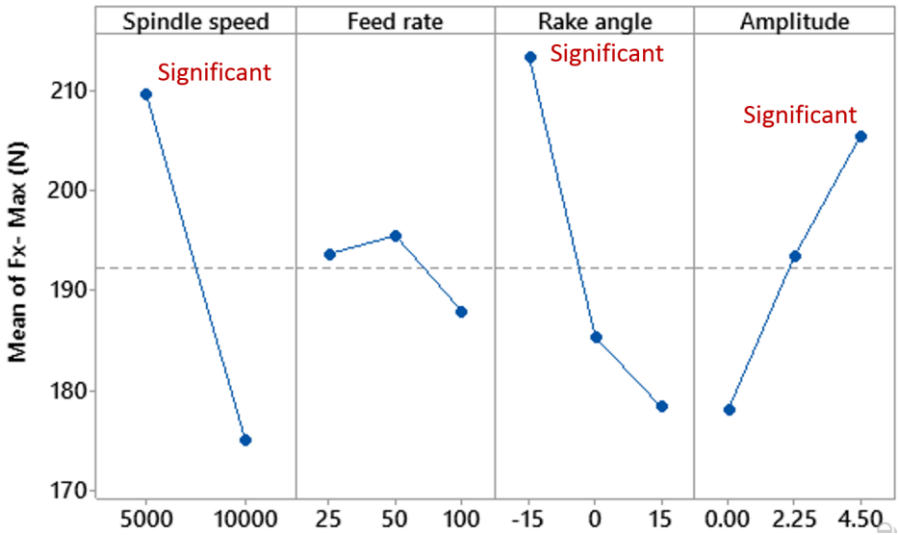

Figure 5: Main effects plot for feed force (Fx-Max)

On the other hand, the rake angles 0° and -15° remove fibers by compression and bending, which require more forces for the cutting process, especially when dealing

with multidirectional laminates, and this all depends on each ply and could also relate to frictional forces associated with different rake angles. However, these forces were found not sensitive to rake angle. There was no significant effect for the interaction between the rake angle and vibration amplitude (CD) on the main cutting force Fx.

Additionally, the oscillation amplitude may has significantly affected the feed force due to the added frictional force to the primary cutting mechanism. Despite the fact that the intermittent cutting of UAM normally allows a separation period between each cutting cycle, this was not the case as the contact with the workpiece was constant since the tool oscillation (z-axis) direction was perpendicular to the feed direction (x-axis). Again, the oscillating setup may have contributed in force and the rise in the amplitude leads adds extra friction force, which in turn increases the feed force, as shown in Figure 5. On the contrary, the feed rate, which reduces the contact time and hence Fx, showed the lowest contribution to a reduced feed force possibly because the end mill possesses a single cutting edge on its circumference and contact time is already reduced.

Regarding the radial force (Fy), the spindle speed (A) was the most significant factor, followed by feed rate (B), amplitude (D), and rake angle (C). The interaction rake angle and amplitude (CD) was not significant, as shown in Figure 6. However, there were interactions between feed rate and amplitude (BD). Therefore, reducing the feed rate and amplitude has a positive effect on the normal force.

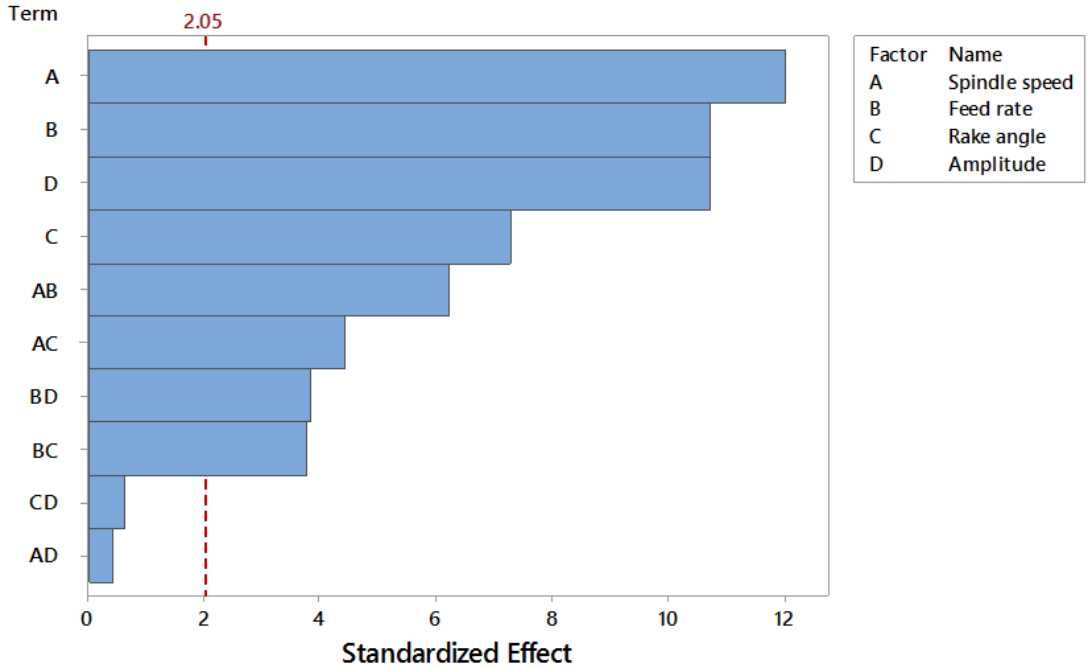

Figure 6: Pareto chart of the standardized effects Fy-Max

It is observed that Fy showed higher values compared to Fx, which is indicative of the dominant frictional load in the machining of CFRPs, even at small depths of cut. The same observation was reported by other researchers [30, 31]. Therefore, the larger the spindle speed, the higher loads add to the process, which increases Fy, as shown in Figure 7.

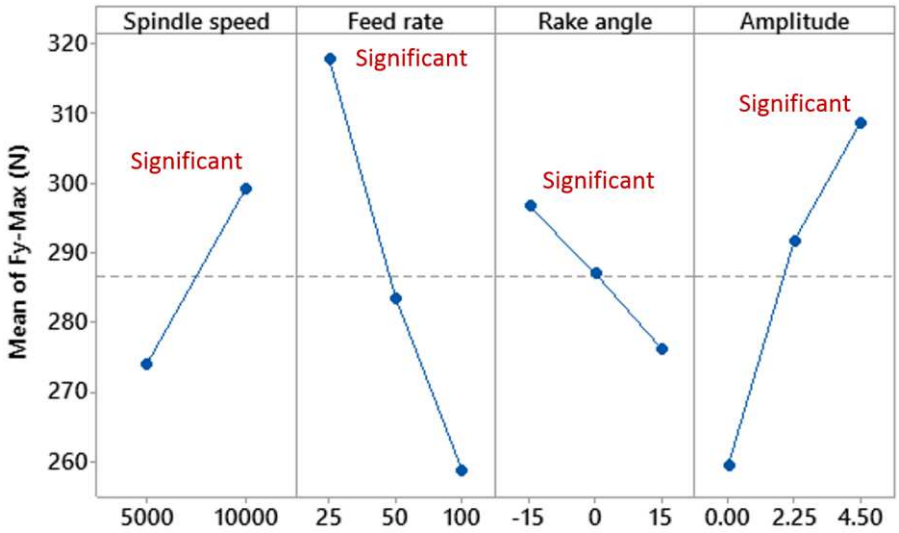

Figure 7: Main effects plot of normal force (Fy-Max)

3.2 Chip temperature

Capture the cutting zone temperature by means of thermal imaging can be difficult. In the present study, the chip temperature generated by tools in the new and worn conditions was captured at the entry (after 10 mm cutting length) and the exit (10 mm before tool disengagement), respectively. Figure 8 shows the lowest (64°C) and highest (107°C) chip temperature, obtained at Test-1 and Test-11, respectively.

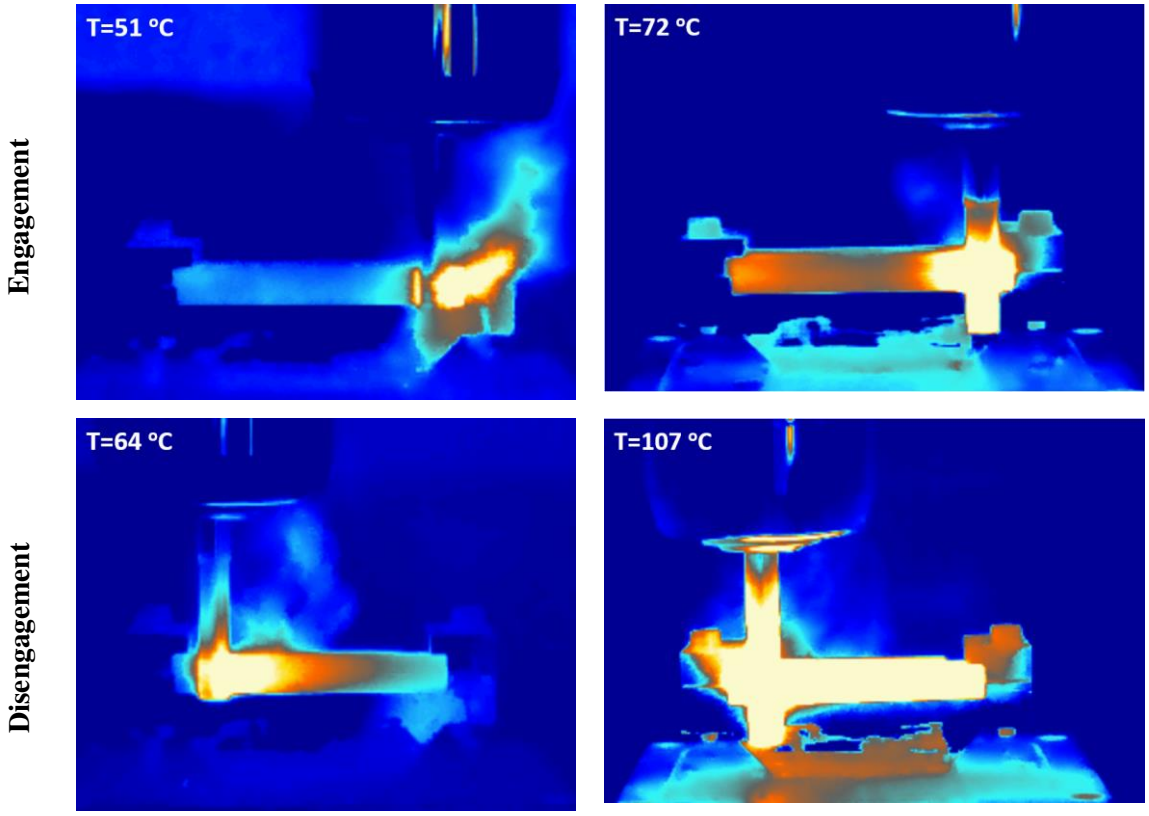

Test1: 5000 rpm (157 m/min), 100 mm/min, 15°, 2.25 µm

Test 11: 10,000 rpm (314 m/min), 25 mm/min, -15°, 4.5 µm

Figure 8: IR images for the lowest (test1) and highest (test 11) chip temperature

It is clear that spindle speed (A) is the most significant factor affecting the chip temperature, followed by feed rate (B), rake angle (C), and amplitude (D) at the tool engagement and disengagement, as shown in Figure 9 and 10, respectively. The contribution of spindle speed is dominant as a result of the excessive friction that generates more heat energy, especially when spindle speed reached 10,000 rpm (314 m/min). On the other hand, the contribution of the other factors increases at tool disengagement owing to the progression of cutting tool wear as the tool progress to cut more length, which in turn accumulates more heat energy.

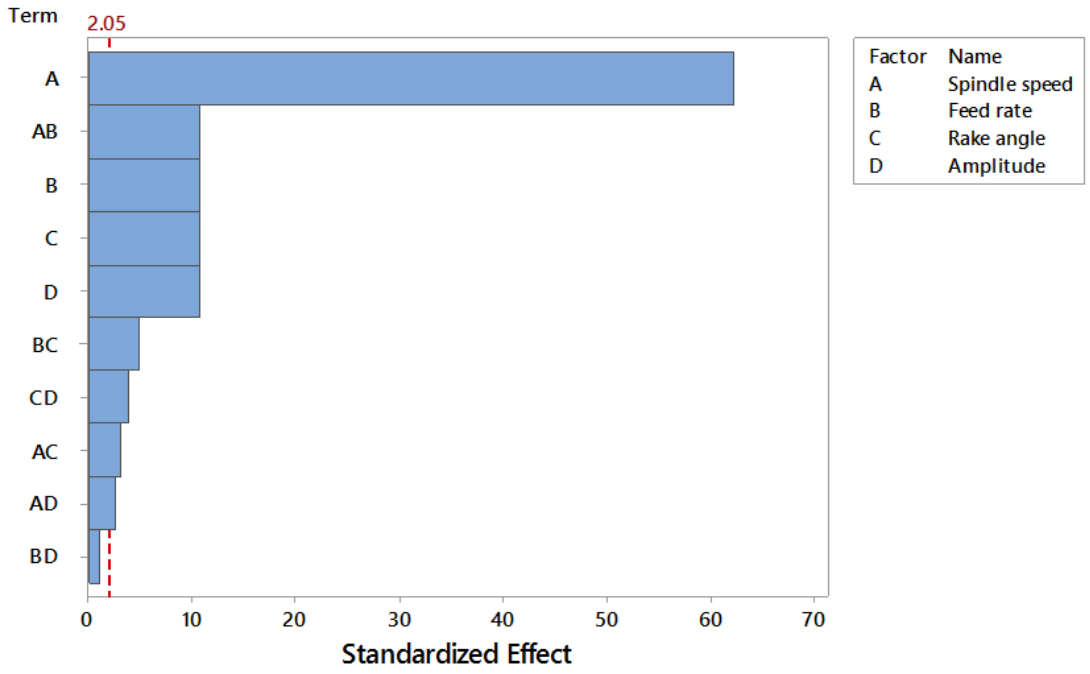

Figure 9: Pareto chart of the standardized effects for chip temperature at tool engagement

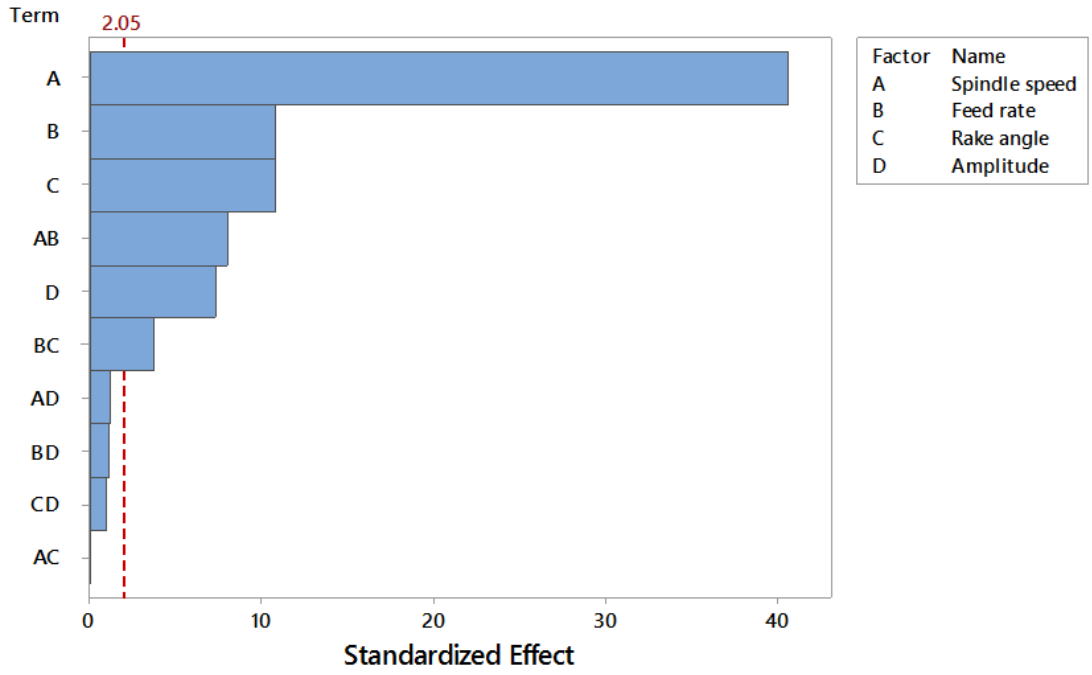

Figure 10: Pareto chart of the standardized effects for chip temperature at tool disengagement

Figures 11 and 12 show the main effects plots with mean values for chip temperature at engagement and disengagement, respectively. When machining this small snapshot CFRP coupon, the increase in feed rate, in this case, reduces the chip temperature as it reduces the contact/rubbing time between the cutting tool and workpiece. Additionally, a positive rake angle (+15) proven another benefit as it reduces the temperature compared to other angles because, as discussed earlier, it facilitates not only chip disposal but also the fractures of the carbon fiber by tension and shear, which reduces the cutting forces. As the vibration amplitude increased, further frictional forces were introduced, a mechanical load translated into an increase in chip temperature. Therefore, UAM is expected to increases cutting temperature compared to conventional cutting (zero amplitude).

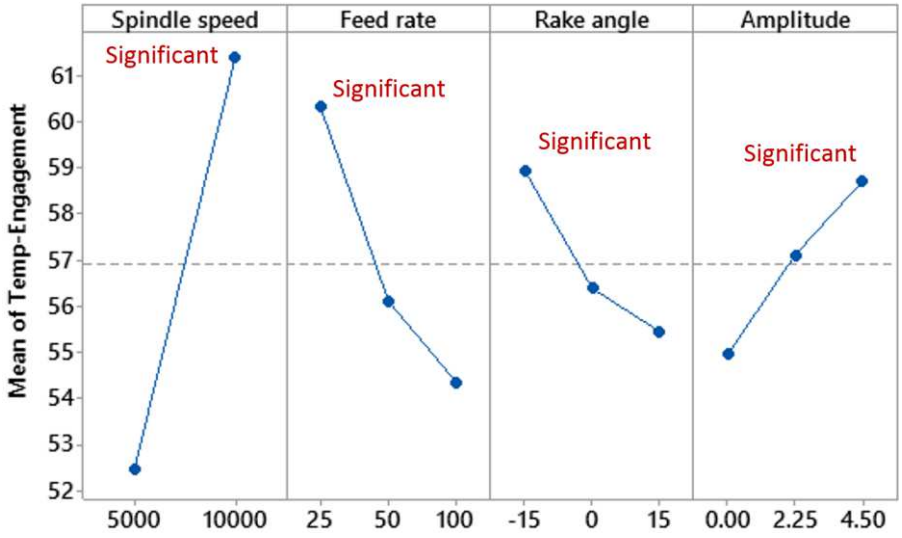

Figure 11: Main effects plot for chip temperature at tool engagement

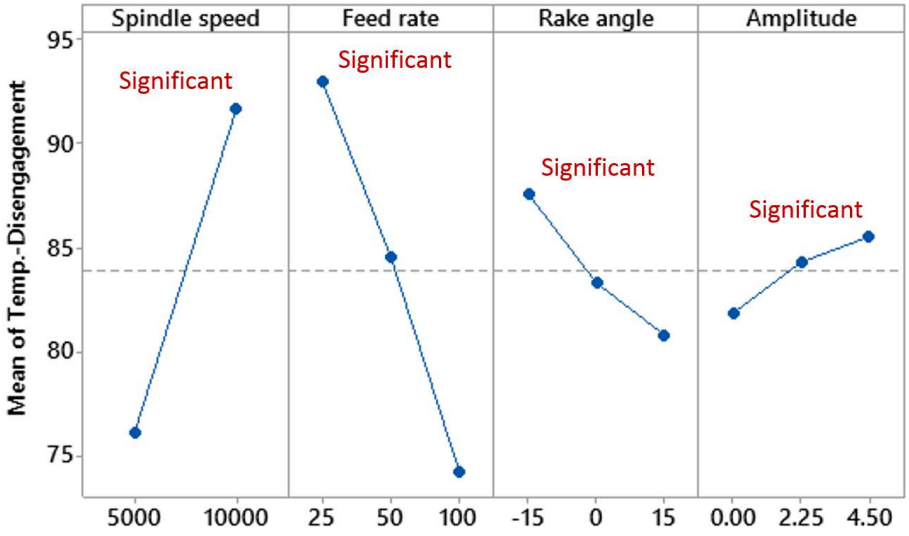

Figure 12: Main effects plot for chip temperature at tool disengagement

3.3 Surface Integrity

Machined surface integrity in terms of quality aspects such as surface roughness and the presence of defects or subsurface damage are useful for the assessment of the cutting process capability. The surface roughness (Ra) was measured at the transversal direction in order to capture the

surface damages across all CFRP plies. Again, the Ra parameters were measured at the same locations, i.e., tool engagement (10 mm) and tool disengagement (70 mm), in order to correlate to wear progression. Figure 13 shows that the rake angle (C) is the most significant factor affecting the surface roughness, followed by feed rate (B) and the interactions AD, AC, and BC.

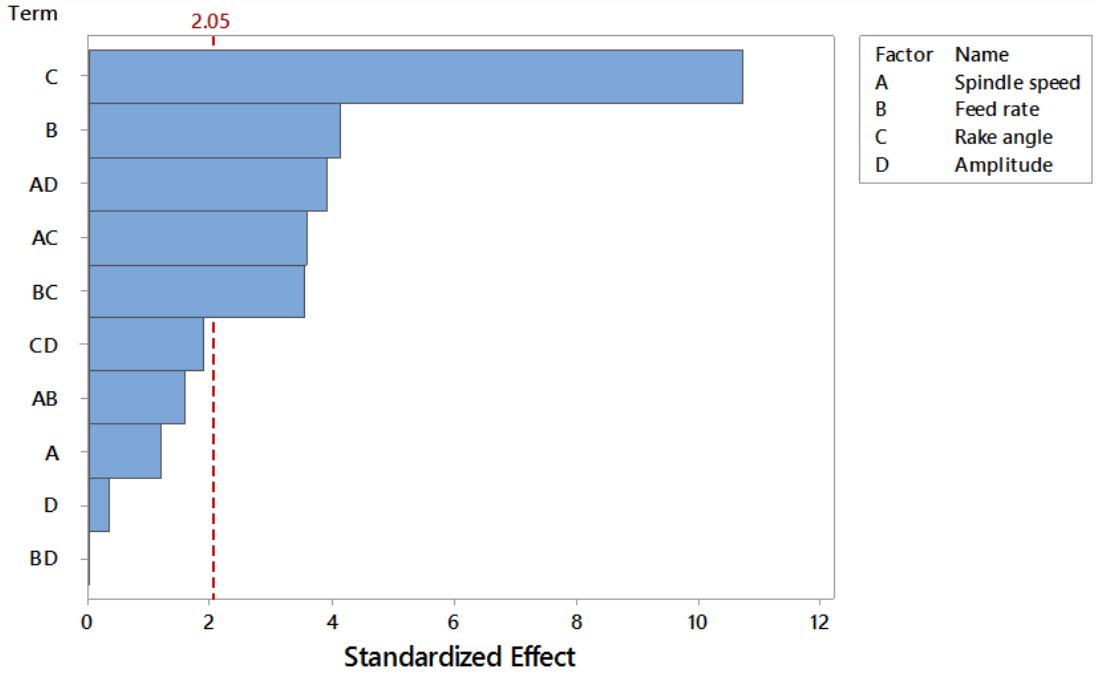

Figure 13: Pareto chart of the standardized effects for Ra at tool engagement

Rake angle plays a role in deciding the chip formation mechanism, which varies depending on the orientation (0°, 45°, 90°, and -45°) of the carbon fibers. Figure 14 shows that a positive rake angle produces cleaner cuts and reduces the surface roughness dramatically compared to 0° and -15°. This is because the positive rake angle applies tension and shear load for fracturing carbon fibers. On the contrary, zero or negative rake angle applies compression and bending or buckling depending on fiber orientation.

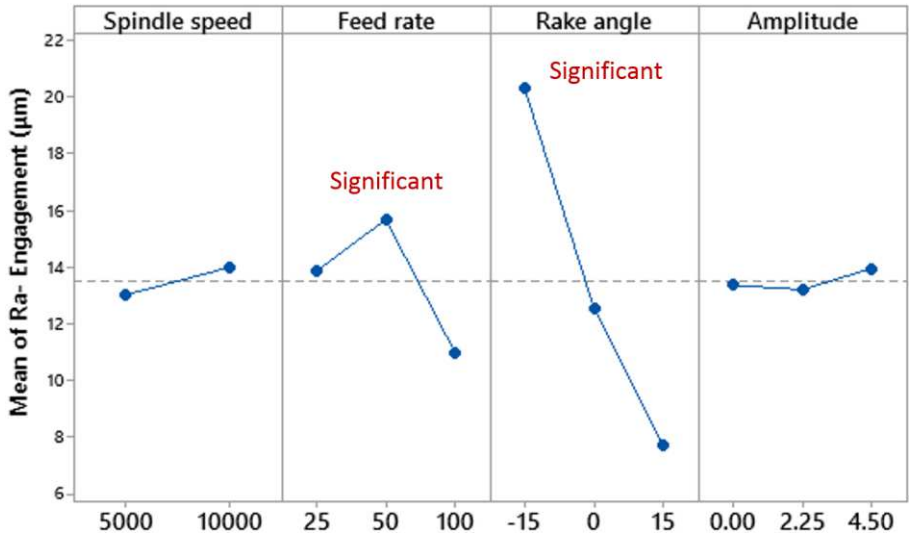

Figure 14: Main effects plot of Ra at tool engagement

It is clearly observed from Figure 15 that subsurface damage, especially in 45° layers, occurs at a rake angle of 0°. Since the fiber fracture occurs by the compressive load, it induces shear across the fiber direction. Then, the interlaminar shear fracture occurred along with the fiber-matrix interface. Spindle speed (A) exhibited minimal contribution to surface roughness. At 10,000 rpm spindle speed, a minute increase in Ra was seen possibly as a result of the elevated cutting temperature, which leads to resin smearing, especially at plies with the orientation 45°, as shown in Figure 15 b). In contrast, figure 16 showed that lowering spindle speed provides better subsurface with minor loss of fiber. The fiber damages occurs when cutting direction inconsistent with the fiber orientation of 45°.

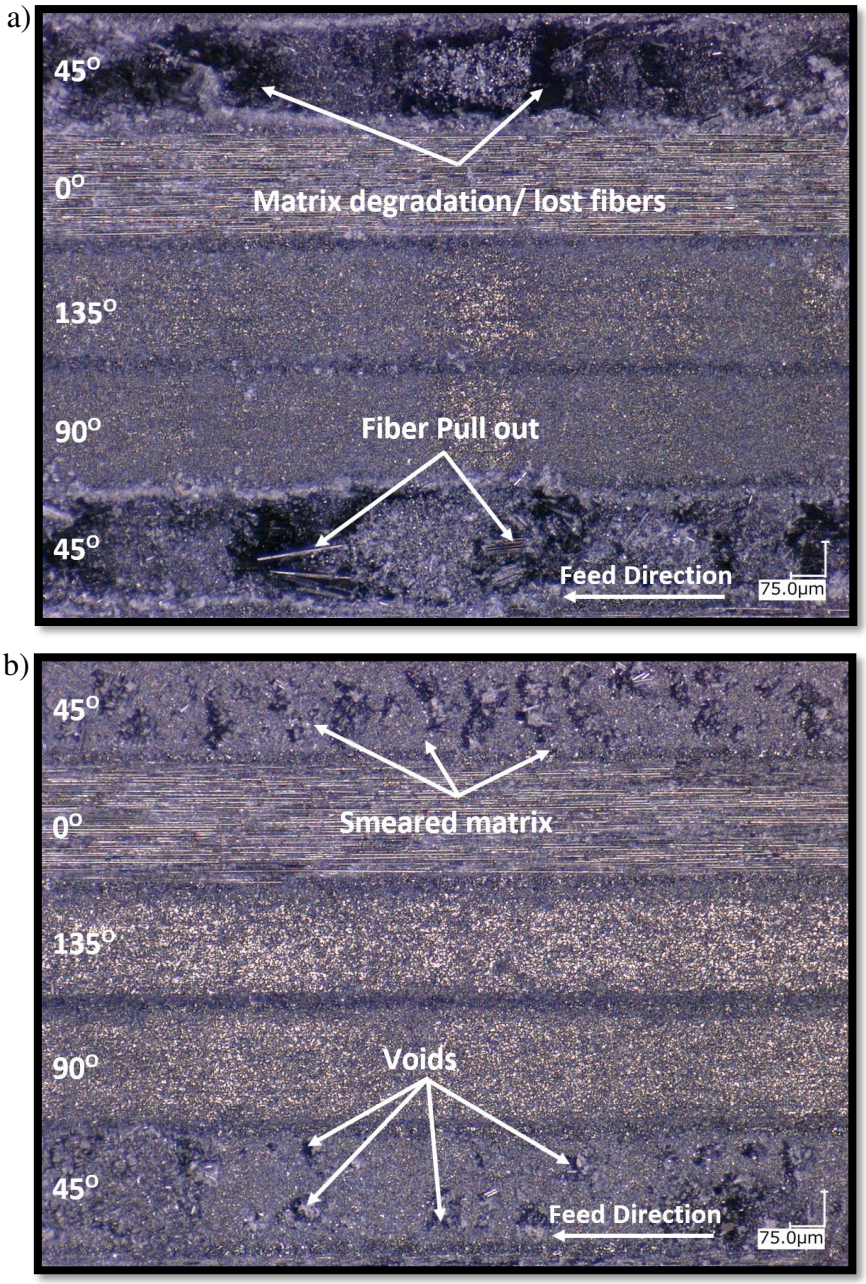

Figure 15: Effect of rake angle on surface quality at conditions of 10,000 rpm, 50 mm/min, 4.5 µm a) rake angle 0° (Test 17) b) rake angle 15° (Test 52)

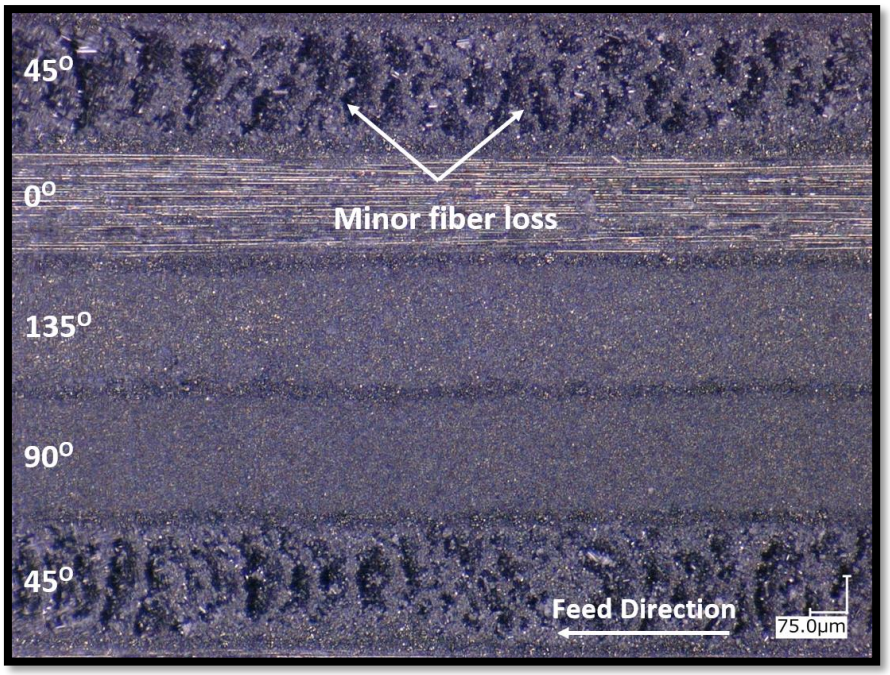

Figure 16: Effect of low spindle speed on surface quality at conditions of 5,000 rpm, 50 mm/min, 4.5 µm, and rake angle 15° (Test 26)

It is evident that the ultrasonic mode slightly increases the Ra at the tool engagement, as shown in Figure 14. An interaction plot, Figure 17, supports the interpretation of this finding such that there is no interaction between the rake angle (C) and amplitude (D). However, it is evident that ultrasonic mode decreased the surface roughness at a positive rake angle (+15 °) and increased it at rake angles of 0° and -15°. In other words, the friction action that occurred at the ultrasonic mode facilitates the fracture of fiber with a +15 rake angle but worsens the situation using 0° and -15° rake angle tools. Again the +15 rake angle is on top of the leader board for better forces, temperature and surface roughness responses at ultrasonic mode.

There existed an interaction between the spindle speed and amplitude (AD). For instance, in ultrasonic mode, the slight increases the Ra at low speed (5000 rpm) could be due to excessive friction introduced leading to a rise in the cutting temperature and consequently resulting in voids and subsurface damages. Furthermore, the increase in spindle speed up to 10,000 rpm elevates the cutting temperature to levels that cause matrix smearing which enhances the surface quality. The temperature should be monitored to avoid further rise beyond the Tg which will increase the risk of matrix degradation or burning. Therefore, increasing spindle speed with the aid of ultrasonic mode can balance or overcome the shortcomings of using a negative rake angle with respect to surface roughness.

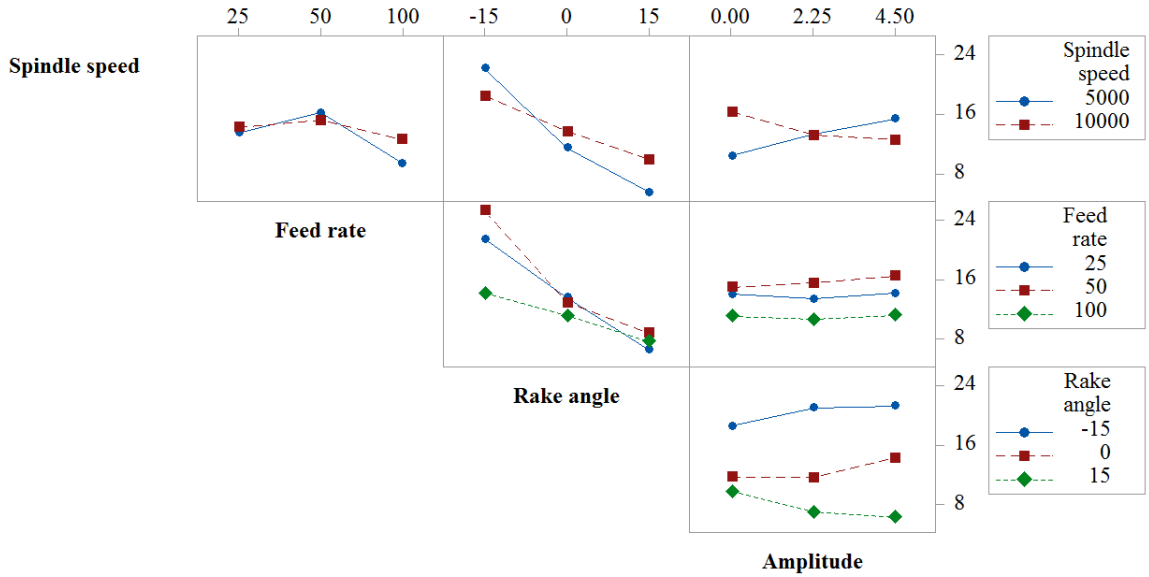

Figure 17: Interaction plot for Ra at tool engagement

Generally, the cutting forces, cutting temperature, and tool wear all increased as the tool advanced and the length of cut increased. Therefore, the ultrasonic mode is assessed before tool disengagement. Although tool wear increases with increasing the cutting length, the increase in spindle speed generates more heat energy that can smear the epoxy resin, and enhance surface finish, see Figure 18. Additionally, within this short sample length, increasing the feed rate is expected to reduce the contact/heating time between the cutting tool and workpiece, which should reflect on better surface integrity [2]. However, there was initial increase, and the feed rate of 50 mm/min was a critical point beyond which the surface roughness decreased. Figures 19 and 20 show a comparison between surfaces obtained at different spindle speeds and feed rates, respectively. Accordingly, the improvement of the surface at higher speeds and feed rates is clear.

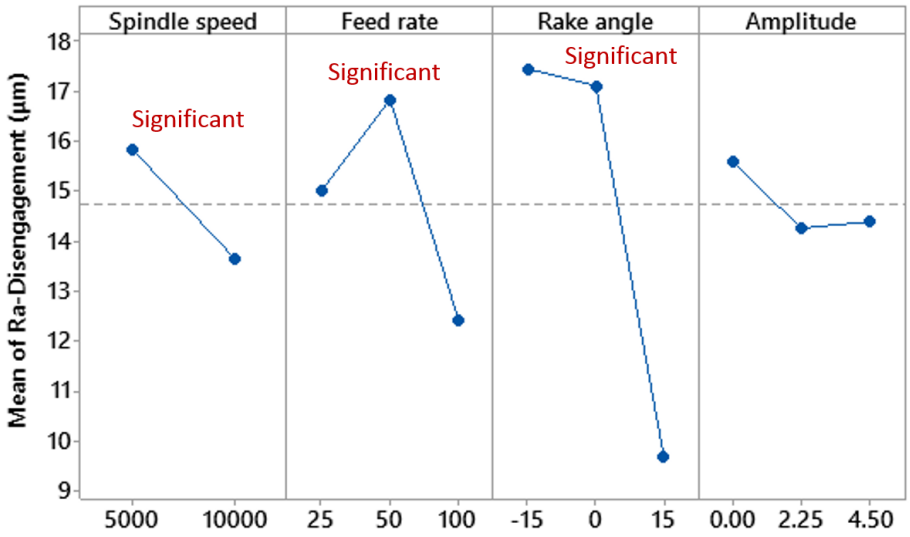

Figure 18: Main effects plot for surface roughness at tool disengagement

(Test 41)
5000 rpm,
100 mm/min,
0°, 4.5 µm

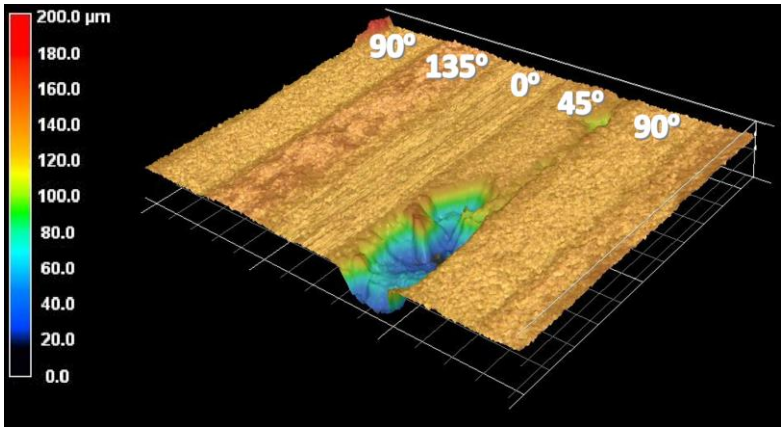

(Test 18)
10,000 rpm,
100 mm/min,
0°, 4.5 µm

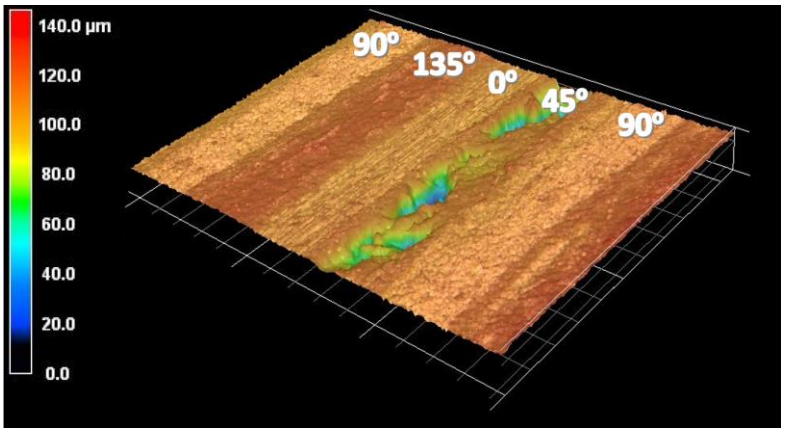

Figure 19: Effect of different spindle speed at tool disengagement

(Test 48)
5000 rpm,
25 mm/min,
15°, 4.5 µm

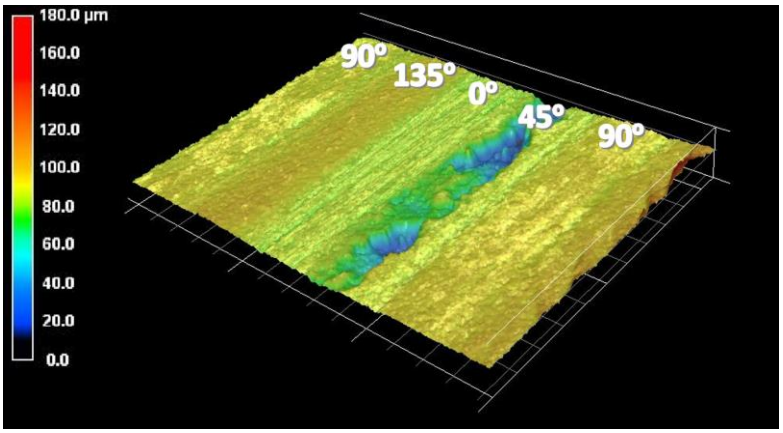

(Test 16)
5000 rpm,
100 m/min,
15°, 4.5 µm

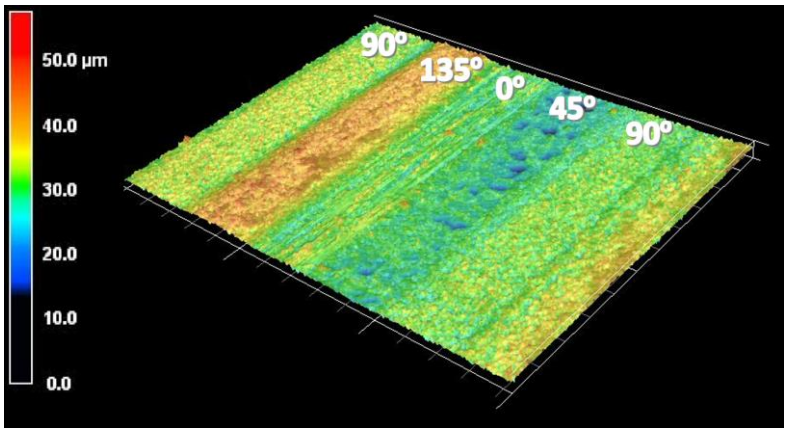

Figure 20: Effect of different feed rate at tool disengagement

When the ultrasonic mode is activated, it can be seen that ultrasonic amplitude improves the surface roughness compared to conventional cutting at tool disengagement. Figure 21 shows the interaction plot for the process parameters. As can be seen, the ultrasonic mode decreases the surface roughness at rake angles of +15° and -15° owing to more efficient cutting action in the presence of ultrasonic mode, which fractures the fibers easily.

On the contrary, the rake angle of 0° was responsible for the deterioration in surface quality at the tool disengagement when the ultrasonic vibration is applied. A similar observation was reported during the orthogonal cutting of graphite/polymer composites [32]. This is mostly because either compression stress imposed by a negative rake angle tool or tensile stresses imposed by a positive rake angle can reduce the surface roughness, and either case will depend on fiber orientation. However, zero rake angle tools are in the middle, which stack with the majority of fiber orientation and provides the worse surface finish, see Figure 22. The surface marks produced in UAM are similar to the conventional but with shallower depth. It is noteworthy that the effect of UAM could have showed greater effect if the direction of oscillation is perpendicular to the surface or if the tool had a helix and this needs to be investigated.

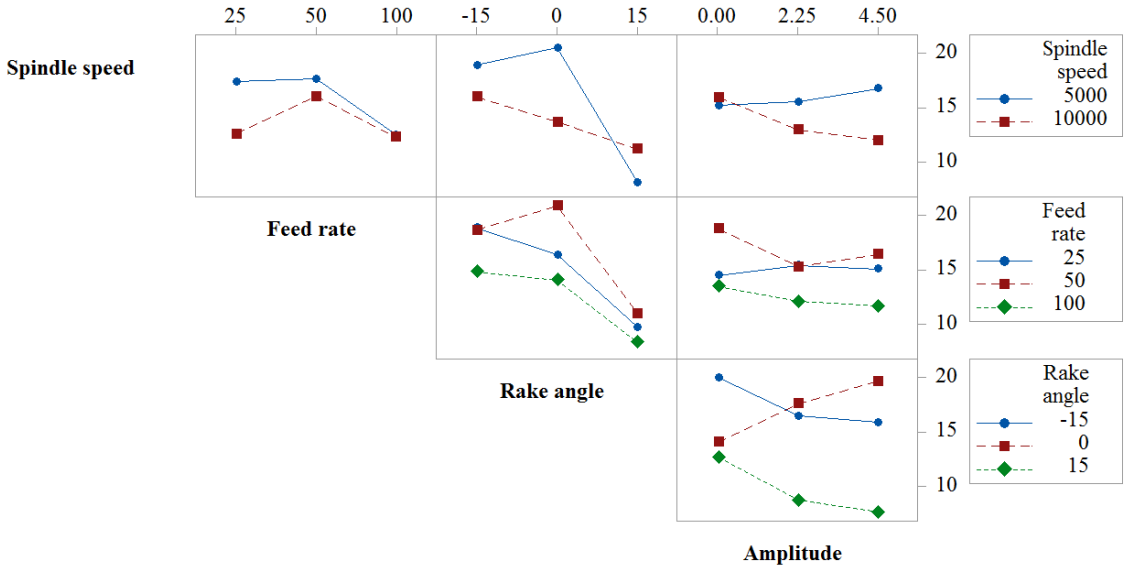

Figure 21: Interaction Plot for the Ra at tool disengagement

(Test24)

10,000 rpm,

50 mm/min, -

15°, 4.5 µm

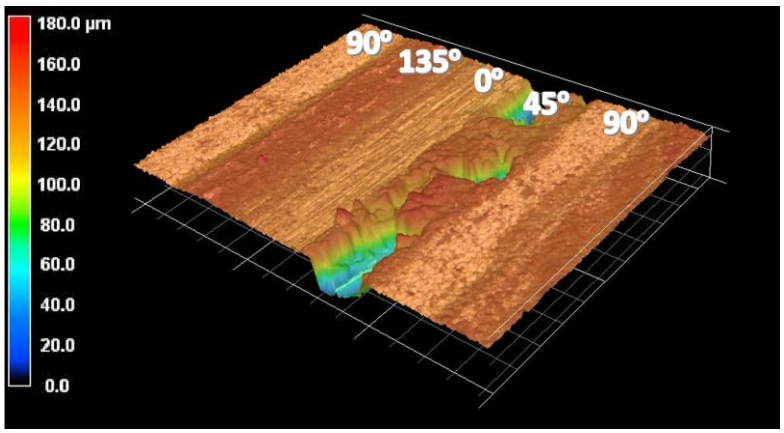

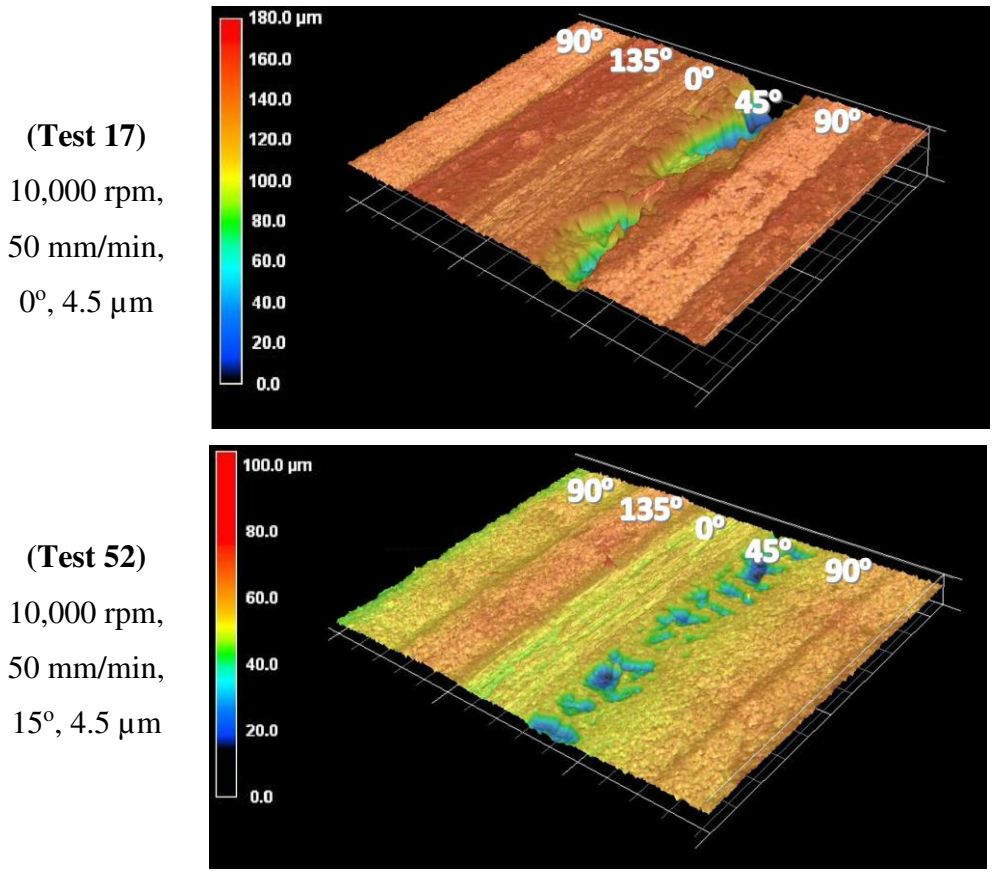

Figure 22: The 3D image of the machined surface using different rake angles at ultrasonic mode

3.4 Tool wear

Understanding the mechanism of tool wear is very important not only from an economic perspective but also for enhancing surface integrity. It is desirable to capture the effect of milling on the edge rounding and retraction when machining CFRP composites. However, the flank wear VB was measured along the cutting edge to represent the tool wear across all CFRP plies (10.4 mm). Generally, for an uncoated carbide tool with an expected high wear rate, the measured wear is lower than an industrial requirement (110 µm) [29] or the commonly used 0.3 mm VB value as a criterion bearing in mind the short cut length used in this evaluation. It is evident that both feed rate (B) and rake angle (C) have a significant effect on tool wear, flowed by amplitude (D), and spindle speed (A), as shown in Figure 23.

As shown in Figure 24, the lower the feed rate, the higher the flank wear rate owing to extended rubbing time between the cutting tool and workpiece at such condition. This exposes the cutting edge to prolonged abrasion/brushing action by the abrasive fibers, which dramatically impair the tool longevity. On the other hand, spindle speed has a significant effect on tool wear. The reduction in the spindle speed can reduce the frictional heat between the cutting tool and workpiece, which in turn reduces cutting temperature and prolong tool life.

Additionally, the negative and zero rake angle tools caused excessive compression load on the cutting tool, which in turn reduces tool life. The ultrasonic assistance exacerbated the cutting condition by adding frictional forces to the compression loads,

which promoted the tool wear and reduced the tool life dramatically. The interaction between feed rate and the rake angle (BC) was significant, owing to their primary contribution to the mechanism of chip removal. This interaction reduces the wear rate at the condition of high feed rates and a positive rake angle, as shown in figure 25. On the contrary, the interactions AB and BD were less significant since they are responsible for increasing cutting temperature. Sharper cutting edge (here tool with +ve rake) have smaller tool angle and are more susceptible to edge rounding/retraction. Therefore, due to the expected loss of the edge and since flank wear is not the dominant form of wear as a result of the brushing action of abrasive fibers it is better to study the form of the edge and use indices other than VB for evaluating the tool wear.

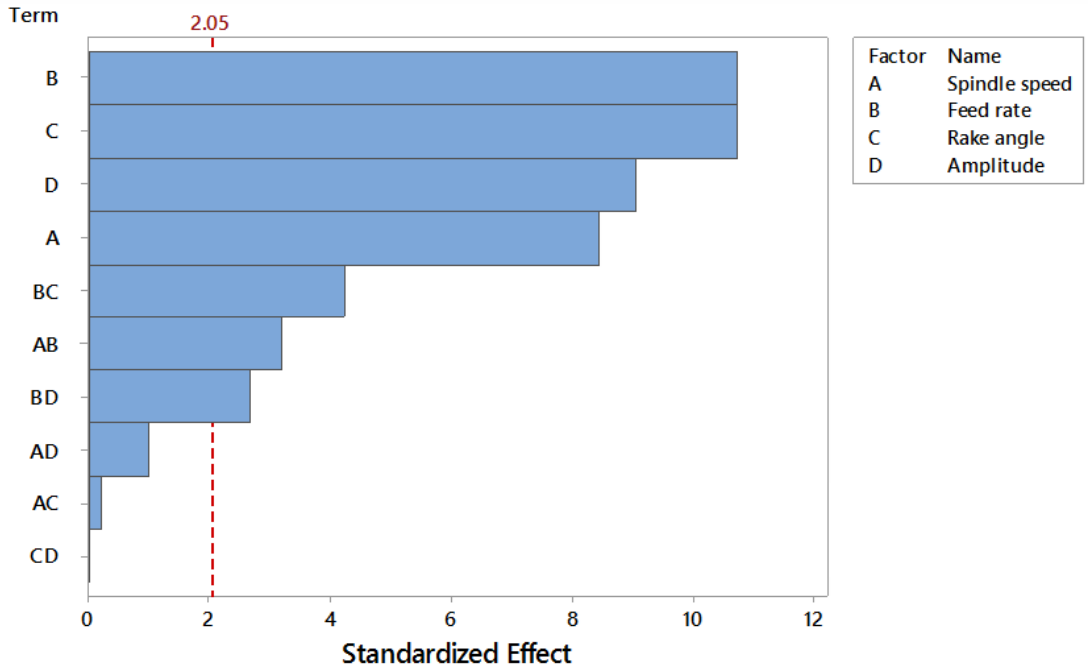

Figure 23: Pareto chart of the standardized effects on tool wear

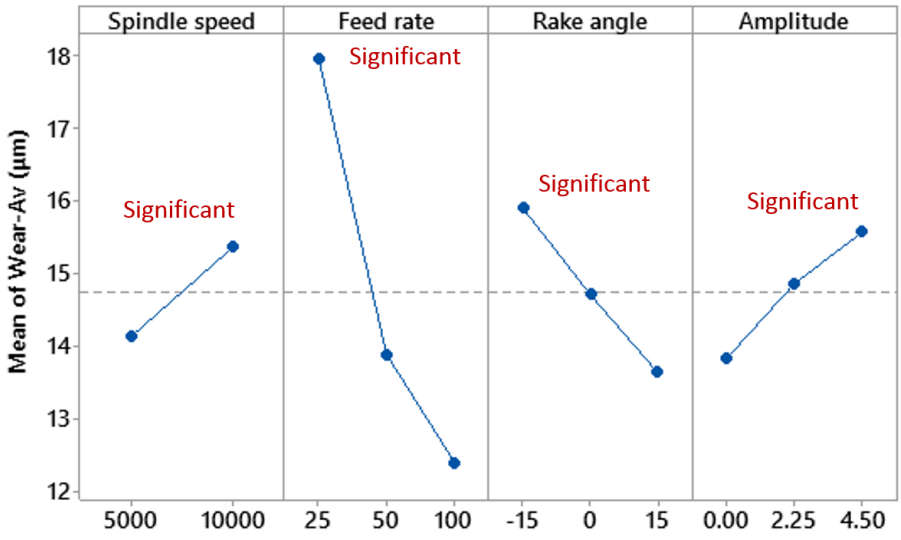

Figure 24: Main effects plot for average tool wear

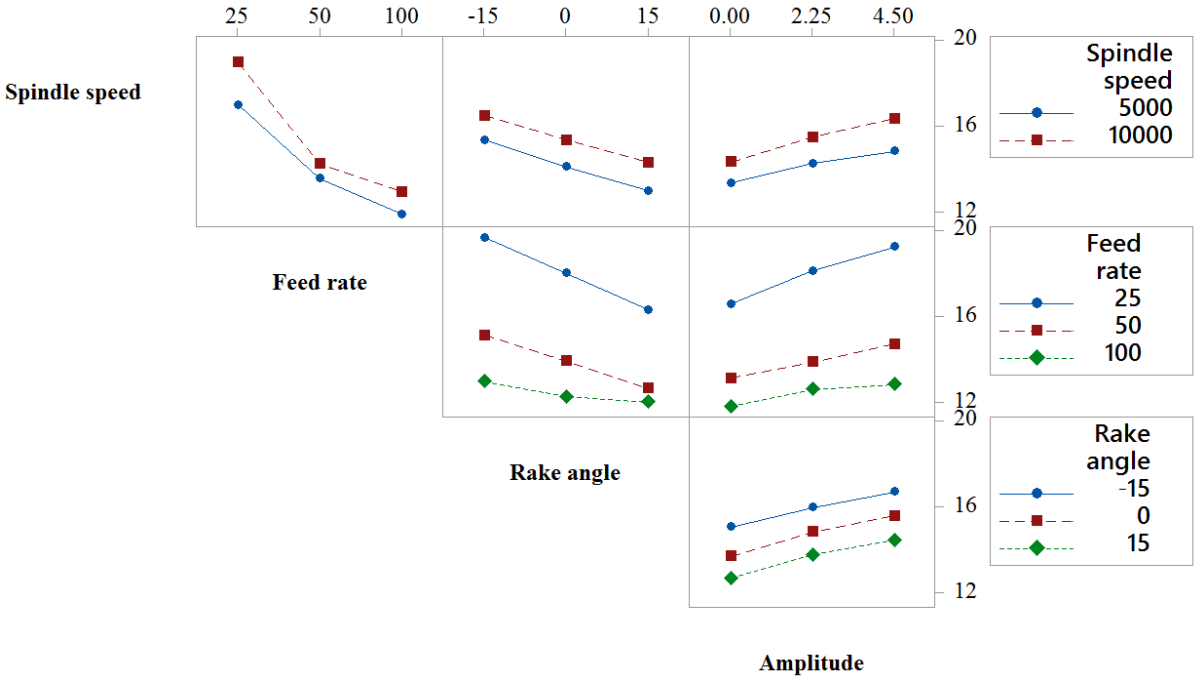

Figure 25: Interaction Plot for the Ra at tool disengagement

4. Conclusion

This article presented an investigation into the effect of tool geometrical features, more specifically having different rake angles, on the surface integrity of multidirectional CFRP laminates during the ultrasonic-assisted edge trimming process. The process parameters are spindle speed, feed rate, rake angle, and the magnitude of amplitude. While the performance characteristics are cutting forces, chip temperature, surface integrity, and tool wear. The findings can be concluded as follows:

- Spindle speed has a significant effect on cutting forces, followed by rake angle, amplitude, and feed rate, owing to their primary contribution to chip formation mechanism. The higher the spindle speed, the smaller chip thickness can be obtained.
- Rake angle changes the stress load that breaks the chips during the cutting process. For instance, a positive rake angle applied tension and shear load for fracturing carbon fibers. On the other hand, zero or negative rake angle applies compression and bending or buckling depending on fiber orientation.
- UAM increases the cutting forces owing to it add friction action to the primary cutting mechanism.
- Chip temperature increase with increasing spindle speed and feed rate because both of them add more friction to the cutting mechanism. The increase in chip temperature could be as advantage for enhancing the surface quality by smear the epoxy resin that can cover the small voids and mechanical damages. However, the temperature should be controlled in order not to exceed the Tg of resin, which in turn lead to resin degradation and reduce the strength of CFRP laminates.
- Surface integrity, at tool disengagement, can be enhanced

using ultrasonic mode. This is mostly because the oscillation motion improves the fracturing of carbon fibers. Moreover, UAM increases the cutting temperature, which in turn smears the epoxy resin and covers small defects/voids.

- UAM improves the cutting performance of a negative rake angle and provides a better surface finish compared to conventional mode.
- Tool wear slightly increases with increasing the spindle speed and amplitude. While it dramatically decreases with increasing feed rate and rake angle.

Acknowledgement

Authors would like to thank the Mission Department of the Ministry of Higher Education in Egypt (MoHE) and Tokyo university of Agriculture and Technology for facilitating the access to Sasahara Lab, to thank OSG Corporation for supplying the tools and to thank Airbus for the material used in this research.

Data availability: The raw/processed data required to reproduce these findings cannot be shared at this time as the data also forms part of an ongoing study.

Compliance with ethical standards

Conflicts of interest The authors declare that they have no conflicts of interest.

Ethical approval N/A.

Consent to participate N/A.

Consent to publish N/A.

Code availability N/A.

References

[1] J. P. Davim and P. Reis, "Damage and dimensional precision on milling carbon fiber-reinforced plastics using design experiments," *Journal of materials processing technology,* vol. 160, pp. 160-167, 2005.

[2] M. El-Hofy, S. Soo, D. Aspinwall, W. Sim, D. Pearson, and P. Harden, "Factors affecting workpiece surface integrity in slotting of CFRP," *Procedia Engineering,* vol. 19, pp. 94-99, 2011.

[3] J. Wang, "Abrasive waterjet machining of polymer matrix composites–cutting performance, erosive process and predictive models," *The International Journal of Advanced Manufacturing Technology,* vol. 15, pp. 757-768, 1999.

[4] M. El-Hofy, M. Helmy, G. Escobar-Palafox, K. Kerrigan, R. Scaife, and H. El-Hofy, "Abrasive water jet machining of multidirectional CFRP laminates," *Procedia Cirp,* vol. 68, pp. 535-540, 2018.

[5] H. Wang, J. Sun, J. Li, L. Lu, and N. Li, "Evaluation of cutting force and cutting temperature in milling carbon fiber-reinforced polymer composites," *The International Journal of Advanced Manufacturing Technology,* vol. 82, pp. 1517-1525, 2016.

[6] J. Y. Sheikh-Ahmad, *Machining of polymer composites* vol. 387355391: Springer, 2009.

[7] M. Ucar and Y. Wang, "End-milling machinability of a carbon fiber reinforced laminated composite," 2005.

[8] Y. G. Wang, X. P. Yan, X. Chen, C. Y. Sun, and G. Liu, "Cutting performance of carbon fiber reinforced plastics using PCD tool," in *Advanced Materials Research*, 2011, pp. 14-18.

[9] D. Wang, M. Ramulu, and D. Arola, "Orthogonal cutting mechanisms of graphite/epoxy composite. Part II: multi-directional laminate," *International Journal of Machine Tools and Manufacture,* vol. 35, pp. 1639-1648, 1995.

[10] X. M. Wang and L. Zhang, "An experimental investigation into the orthogonal cutting of unidirectional fibre reinforced plastics," *International journal of machine tools and manufacture,* vol. 43, pp. 1015-1022, 2003.

[11] P. Cao, Z. Zhu, D. Buck, X. Guo, M. Ekevad, and X. A. Wang, "Effect of rake angle on cutting performance during machining of stone-plastic composite material with polycrystalline diamond cutters," *Journal of Mechanical Science and Technology,* vol. 33, pp. 351-356, 2019.

[12] M. Henerichs, R. Voss, F. Kuster, and K. Wegener, "Machining of carbon fiber reinforced plastics: Influence of tool geometry and fiber orientation on the machining forces," *CIRP Journal of Manufacturing Science and Technology,* vol. 9, pp. 136-145, 2015.

[13] A. Faraz, D. Biermann, and K. Weinert, "Cutting edge rounding: An innovative tool wear criterion in drilling CFRP composite laminates," *International Journal of Machine Tools and Manufacture,* vol. 49, pp. 1185-1196, 2009.

[14] P. Ghidossi, M. El Mansori, and F. Pierron, "Edge machining effects on the failure of polymer matrix composite coupons," *Composites Part A: Applied Science and Manufacturing,* vol. 35, pp. 989-999, 2004.

[15] S. Gara and O. Tsoumarev, "Effect of tool geometry on surface roughness in slotting of CFRP," *The International Journal of Advanced Manufacturing Technology,* vol. 86, pp. 451-461, 2016.

[16] A. S. Jahromi and B. Bahr, "An analytical method for predicting cutting forces in orthogonal machining of unidirectional composites," *Composites Science and Technology,* vol. 70, pp. 2290-2297, 2010.

[17] M. O. Helmy, M. El-Hofy, and H. El-Hofy, "Effect of cutting fluid delivery method on ultrasonic assisted edge trimming of multidirectional CFRP composites at different machining conditions," *Procedia CIRP,* vol. 68, pp. 450-455, 2018.

[18] M. O. Helmy, M. El-Hofy, and H. El-Hofy, "Influence of process parameters on the ultrasonic assisted edge trimming of aerospace CFRP laminates using MQL," *International Journal of Machining and Machinability of Materials,* vol. 22, pp. 349-373, 2020.

[19] K. A. Calzada, S. G. Kapoor, R. E. DeVor, J. Samuel, and A. K. Srivastava, "Modeling and interpretation of fiber orientation-based failure mechanisms in machining of carbon fiber-reinforced polymer composites," *Journal of Manufacturing Processes,* vol. 14, pp. 141-149, 2012.

[20] D. Wang, M. Ramulu, and D. Arola, "Orthogonal cutting mechanisms of graphite/epoxy composite. Part I: unidirectional laminate," *International Journal of Machine Tools and Manufacture,* vol. 35, pp. 1623-1638, 1995.

[21] A. S. Jahromi, B. Bahr, and K. K. Krishnan, "An analytical method for predicting damage zone in orthogonal machining of unidirectional composites," *Journal of Composite Materials,* vol. 48, pp. 3355-3365, 2014.

[22] F.-j. Wang, J.-w. Yin, J.-w. Ma, Z.-y. Jia, F. Yang, and B. Niu, "Effects of cutting edge radius and fiber cutting angle on the cutting-induced surface damage in machining of unidirectional CFRP composite laminates," *The International Journal of Advanced Manufacturing Technology,* vol. 91, pp. 3107-3120, 2017.

[23] A. Mkaddem, I. Demirci, and M. El Mansori, "A micro–macro combined approach using FEM for modelling of machining of FRP composites: Cutting forces analysis," *Composites Science and Technology,* vol. 68, pp. 3123-3127, 2008.

[24] J. Sheikh-Ahmad, M. El-Hofy, F. Almaskari, K. Kerrigan, and Y. Takikawa, "The evolution of cutting forces during slot milling of unidirectional carbon fiber reinforced polymer (UD-CFRP) composites," *Procedia CIRP,* vol. 85, pp. 127-132, 2019.

[25] J. Sheikh-Ahmad, F. Almaskari, and M. El-Hofy, "Characterization of the cutting forces and friction behavior in machining UD-CFRP using slot milling test," *The International Journal of Advanced Manufacturing Technology,* pp. 1-13, 2021.

[26] M. G. Nik, M. R. Movahhedy, and J. Akbari, "Ultrasonic-assisted grinding of Ti6Al4V alloy," *Procedia Cirp,* vol. 1, pp. 353-358, 2012.

[27] Z. Jian-Hua, Z. Yan, T. Fu-Qiang, Z. Shuo, and G. Lan-Shen, "Kinematics and experimental study on ultrasonic vibration-assisted micro end grinding of silica glass," *The International Journal of Advanced Manufacturing Technology,* vol. 78, pp. 1893-1904, 2015.

[28] V. A. Phadnis, A. Roy, and V. V. Silberschmidt, "A finite element model of ultrasonically assisted drilling in carbon/epoxy composites," *Procedia Cirp,* vol. 8, pp. 141-146, 2013.

[29] N. F. H. Abd Halim, H. Ascroft, and S. Barnes, "Analysis of tool wear, cutting force, surface roughness and machining temperature during finishing operation of ultrasonic assisted milling (UAM) of carbon fibre reinforced plastic (CFRP)," *Procedia engineering,* vol. 184, pp. 185-191, 2017.

[30] K. Colligan and M. Ramulu, "Edge trimming of graphite/epoxy with diamond abrasive cutters," 1999.

[31] S. L. Soo, I. S. Shyha, T. Barnett, D. K. Aspinwall, and W.-M. Sim, "Grinding performance and workpiece integrity when superabrasive edge routing carbon fibre reinforced plastic (CFRP) composites," *CIRP annals,* vol. 61, pp. 295-298, 2012.

[32] D. Yang, Z. Wan, P. Xu, and L. Lu, "Rake Angle Effect on a Machined Surface in Orthogonal Cutting of Graphite/Polymer Composites," *Advances in Materials Science and Engineering,* vol. 2018, 2018.

Figures

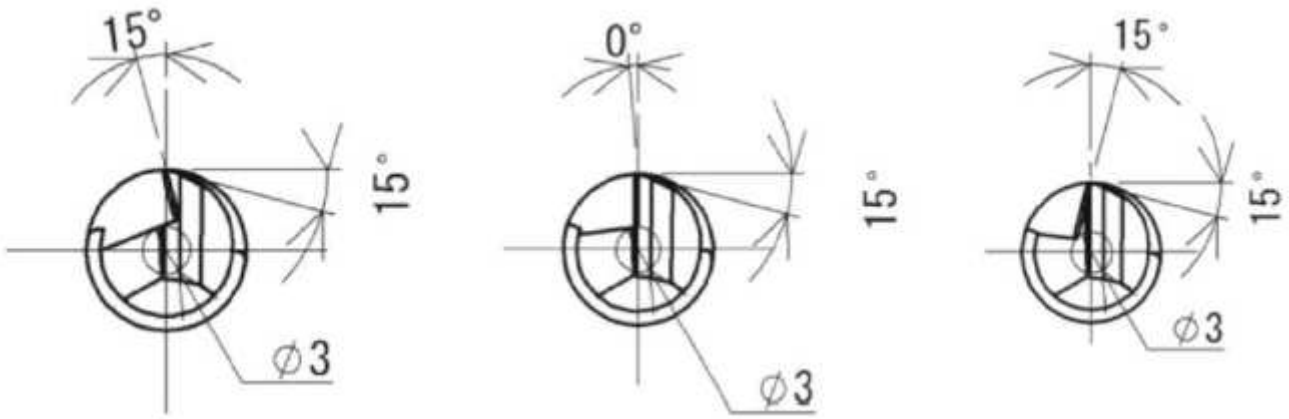

Figure 1

Three different rake angles (15o, 0o, and -15o) for single flute end mill

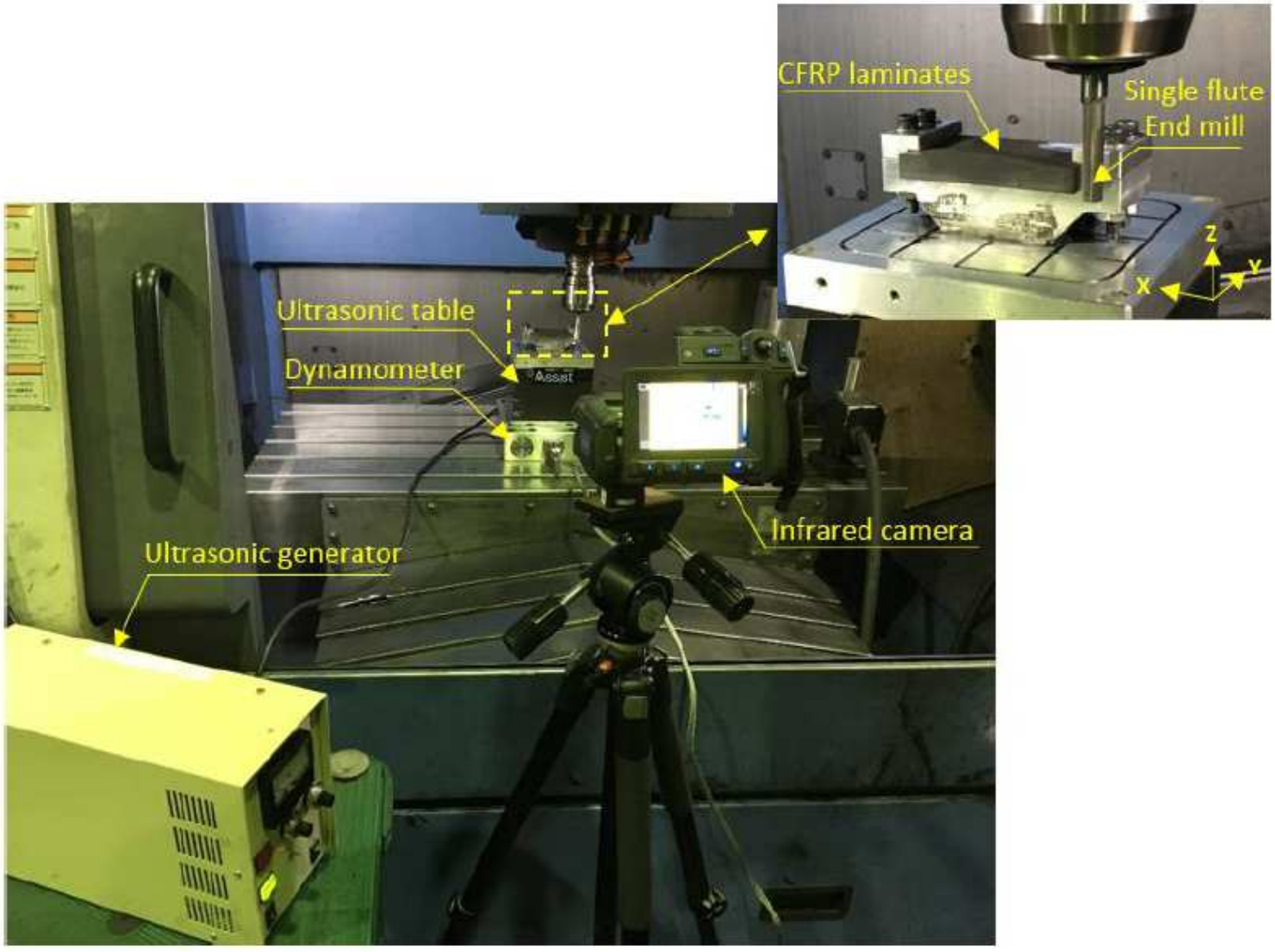

Figure 2

Experimental setup for ultrasonic-assisted edge trimming of CFRP using a defined tool geometry

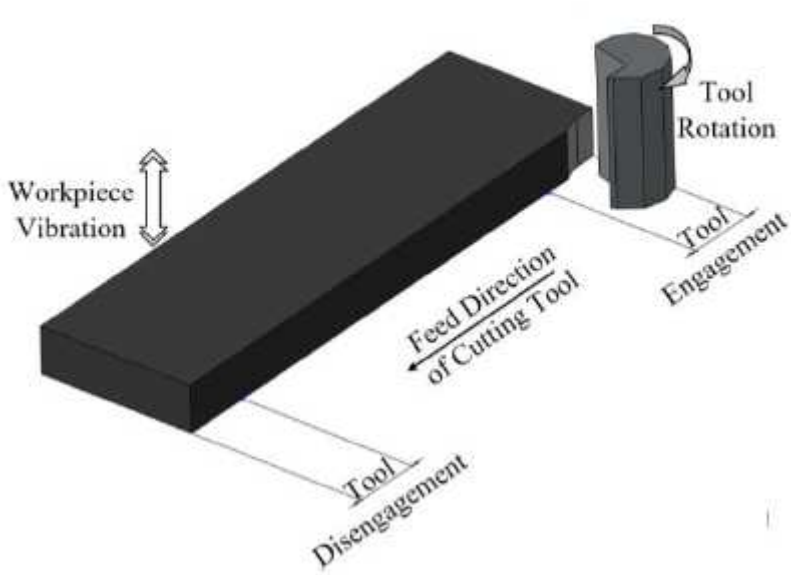

Figure 3

Schematic of ultrasonic-assisted edge trimming of CFRP laminates The variation of average flank wear (VB) was measured along the entire cutting thickness (10.4 mm) was then averaged to represent the tool wear across all CFRP plies.

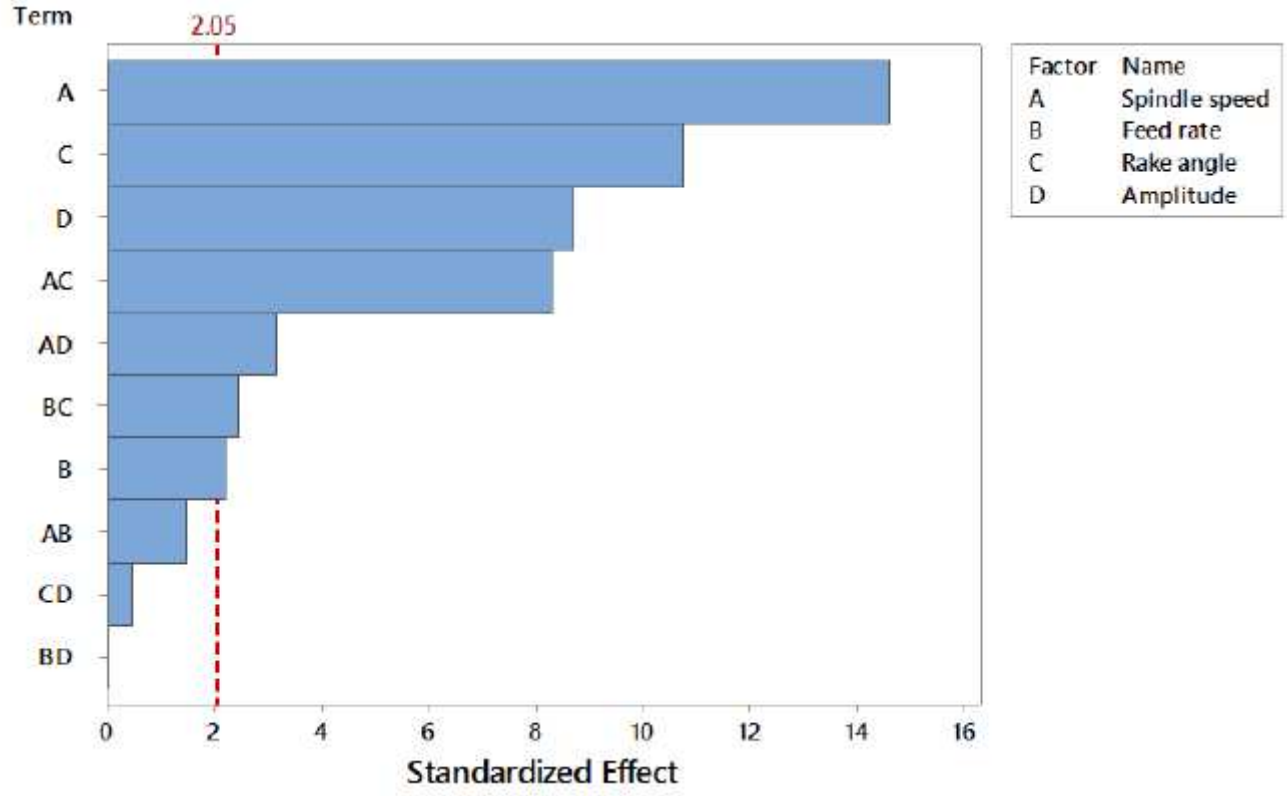

Figure 4

Pareto chart of the standardized effects Fx-Max

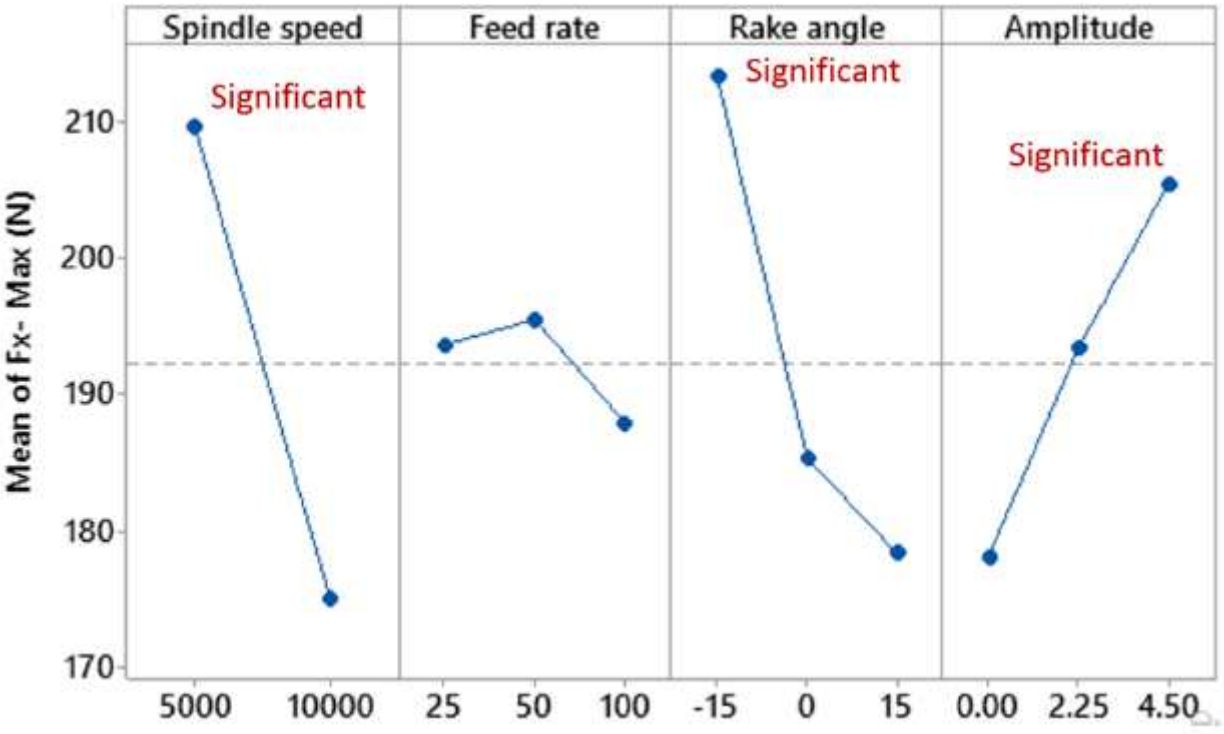

Figure 5

Main effects plot for feed force (Fx-Max)

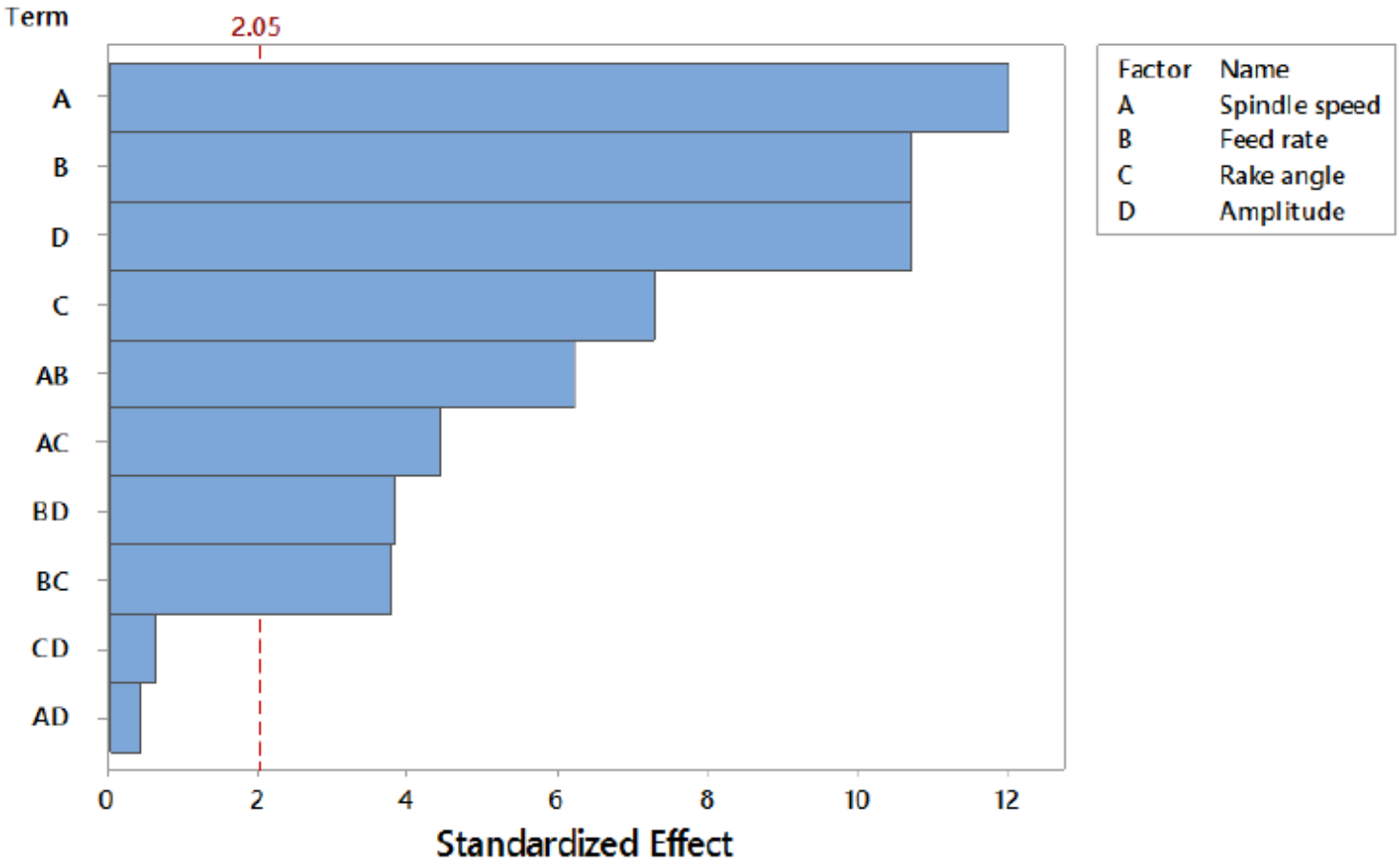

Figure 6

Pareto chart of the standardized effects Fy-Max

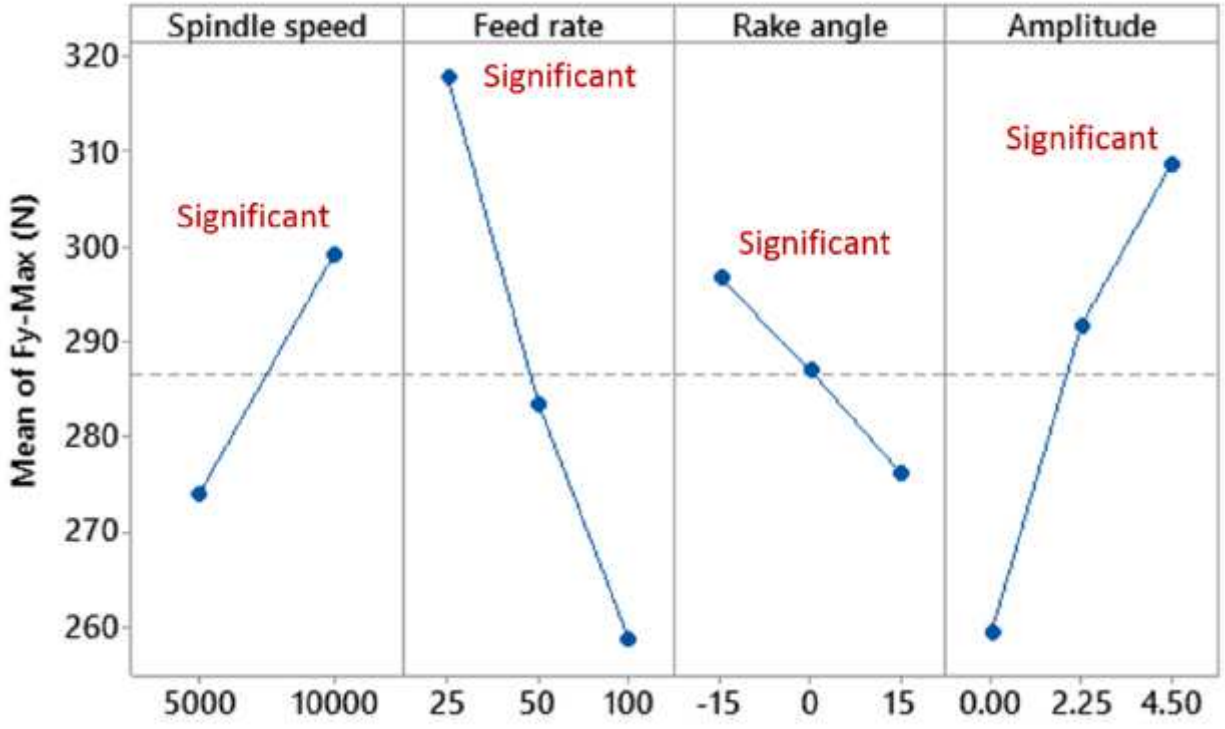

Figure 7

Main effects plot of normal force (Fy-Max)

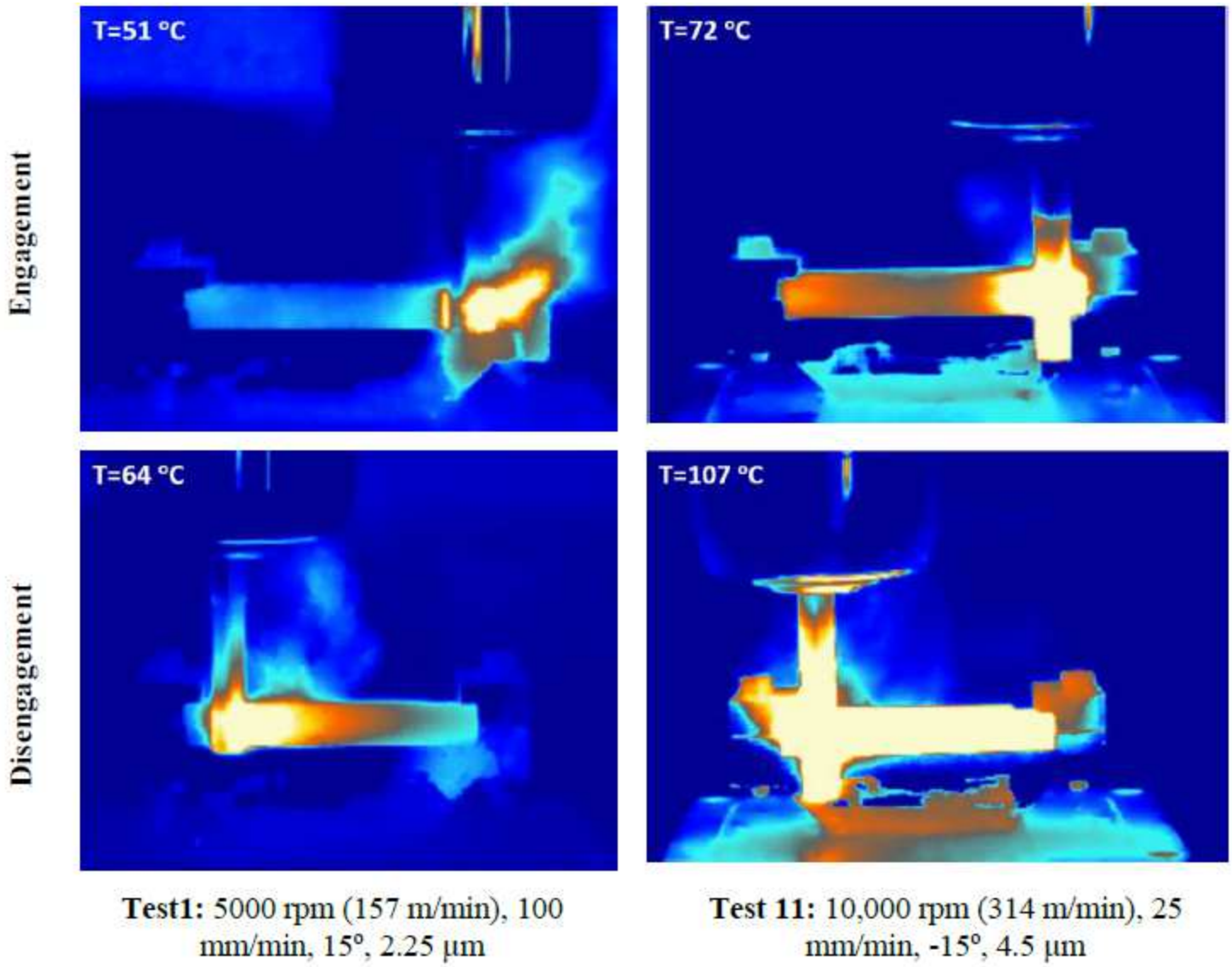

Figure 8

IR images for the lowest (test1) and highest (test 11) chip temperature

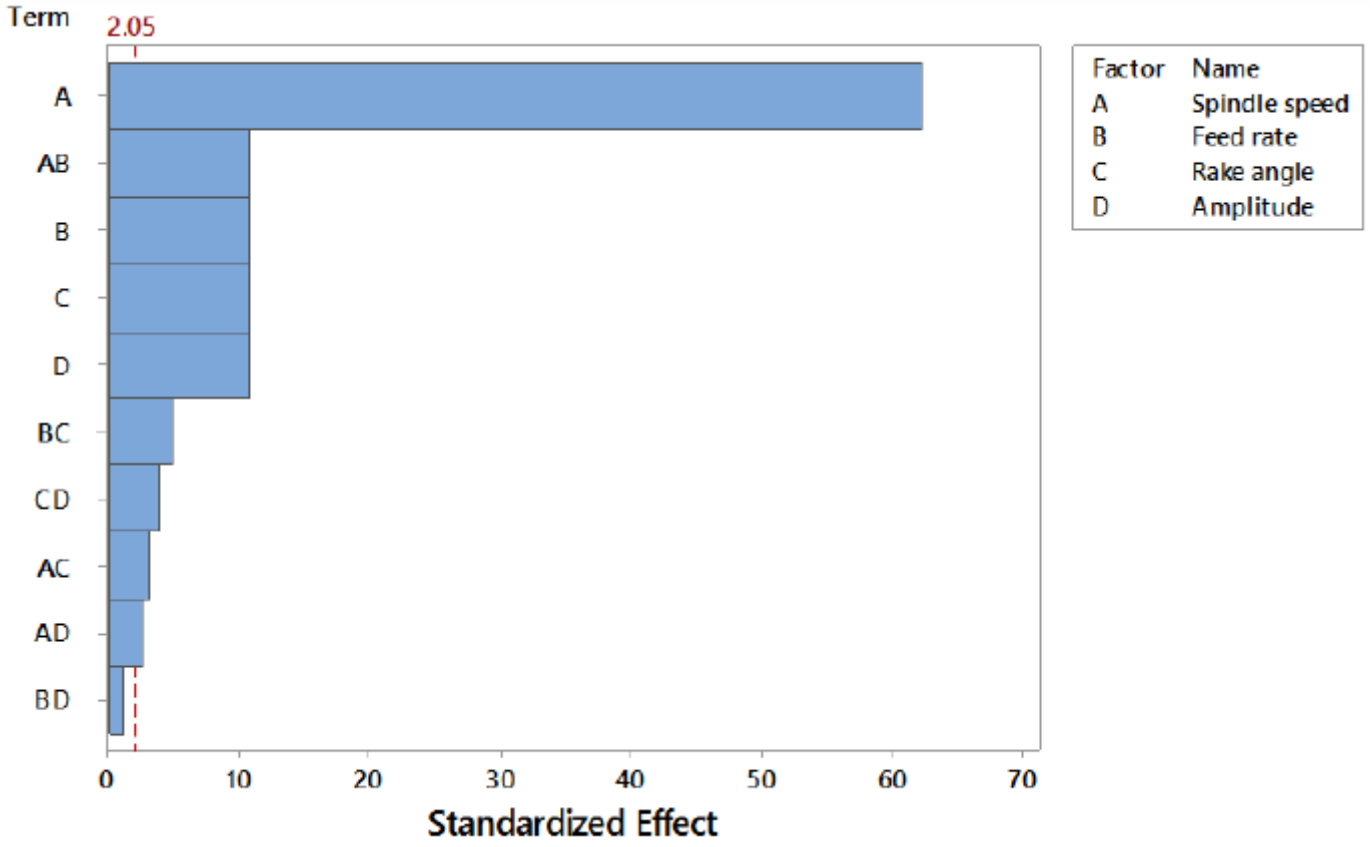

Figure 9

Pareto chart of the standardized effects for chip temperature at tool engagement

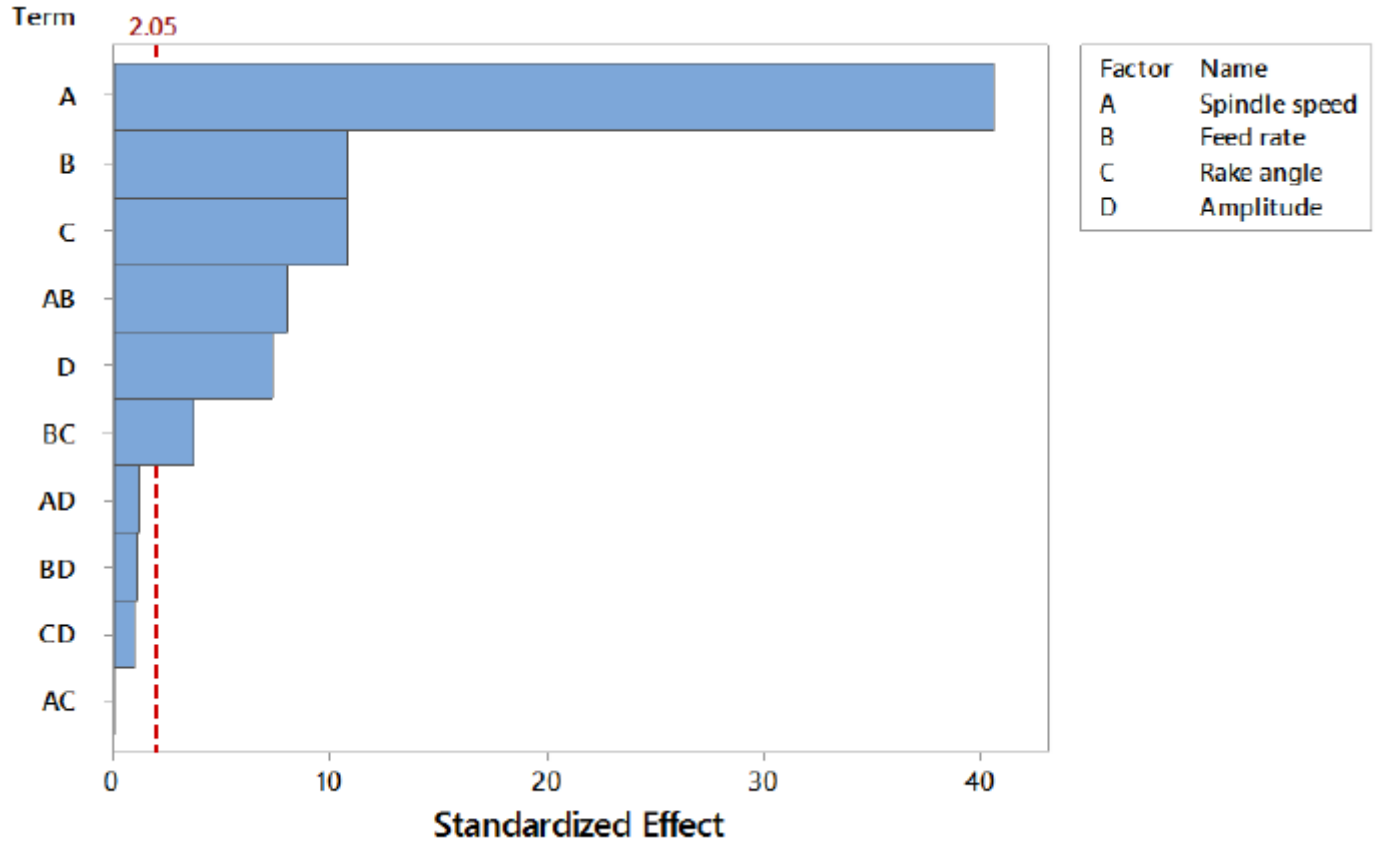

Figure 10

Pareto chart of the standardized effects for chip temperature at tool disengagement

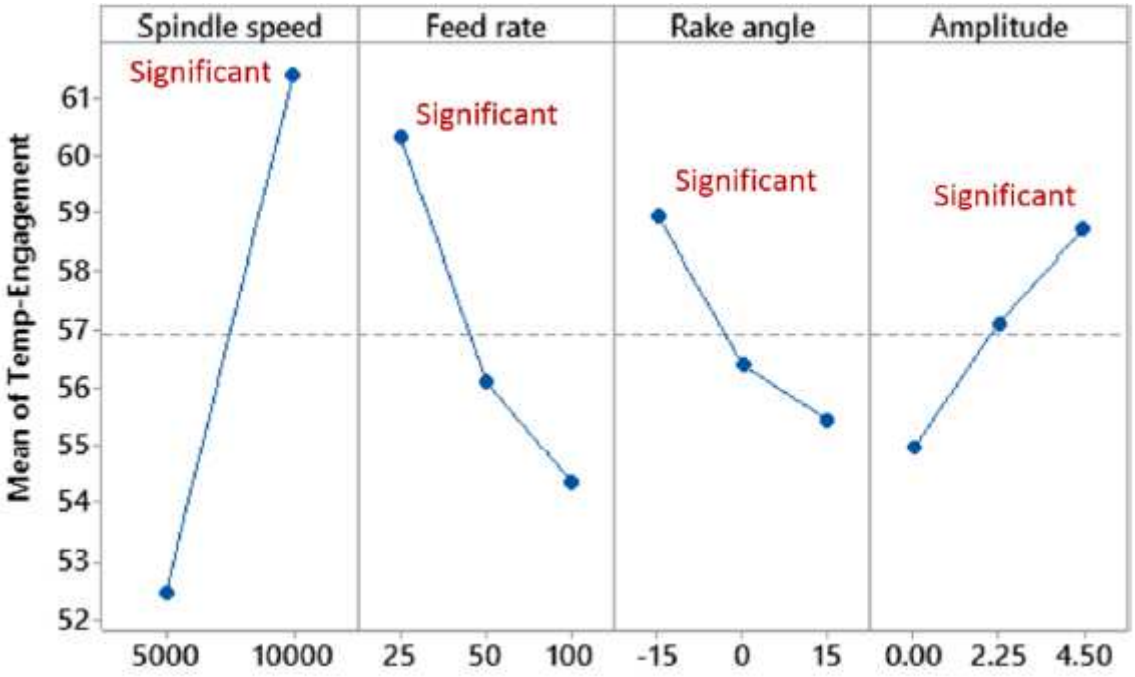

Figure 11

Main effects plot for chip temperature at tool engagement

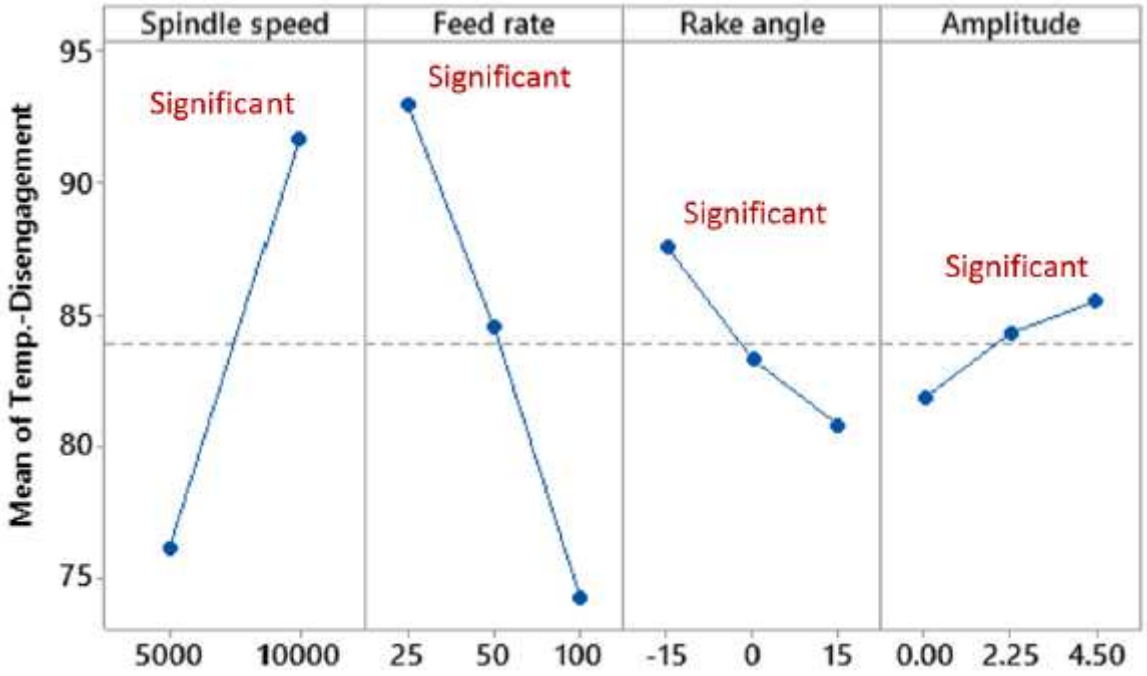

Figure 12

Main effects plot for chip temperature at tool disengagement

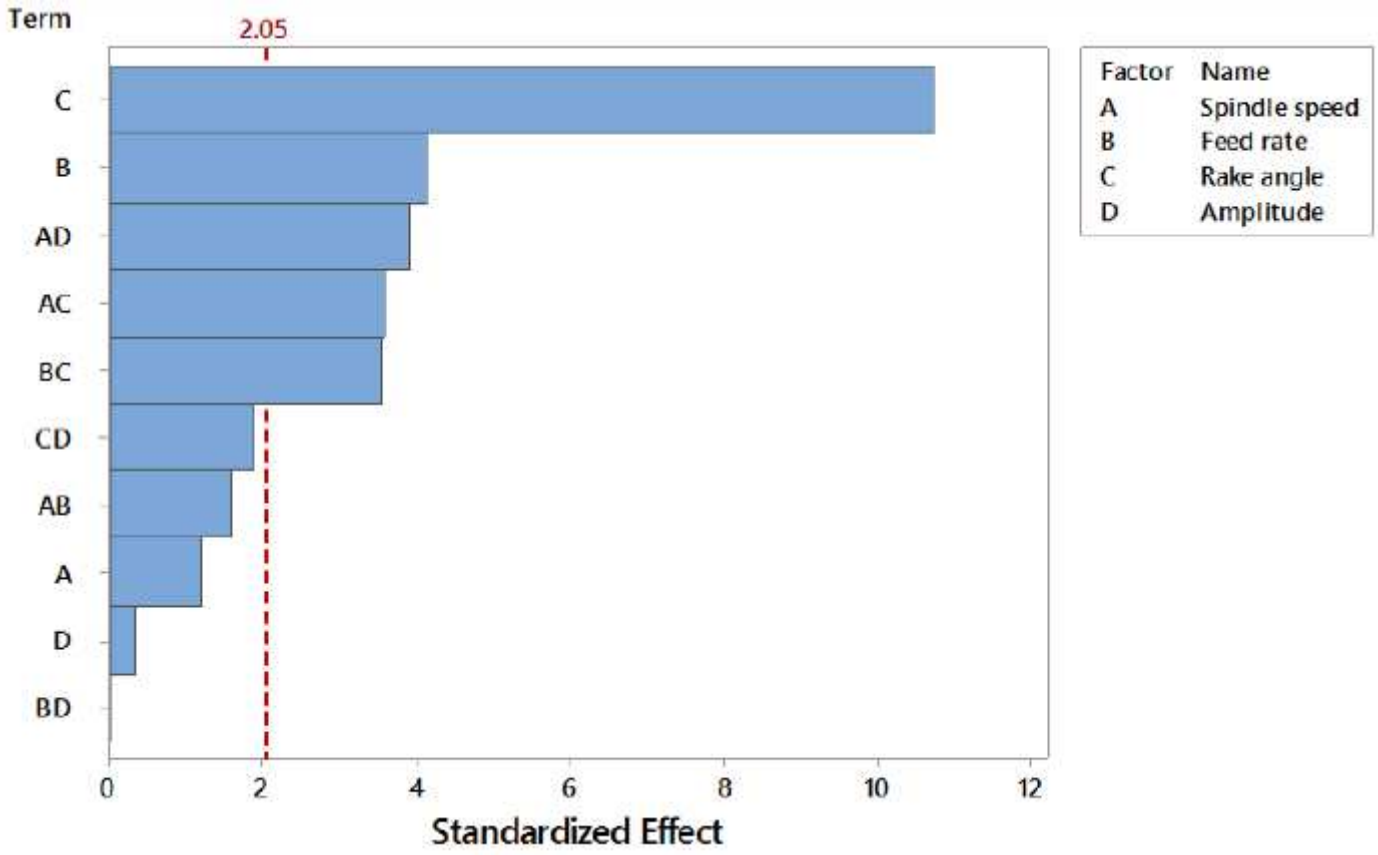

Figure 13

Pareto chart of the standardized effects for Ra at tool engagement

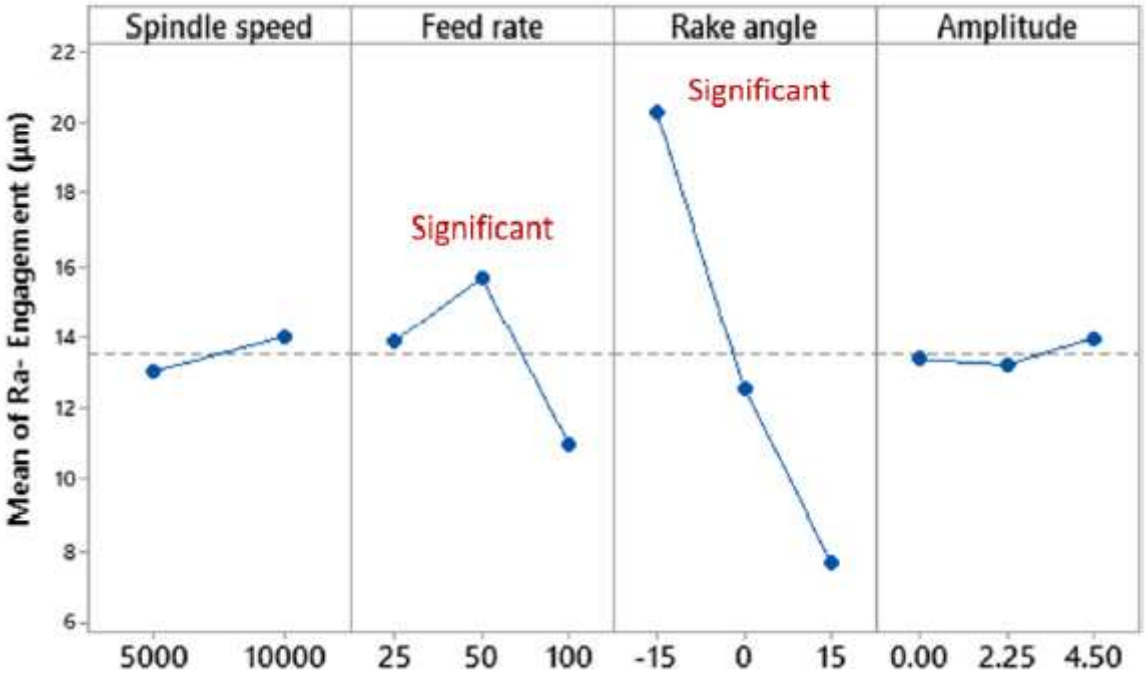

Figure 14

Main effects plot of Ra at tool engagement

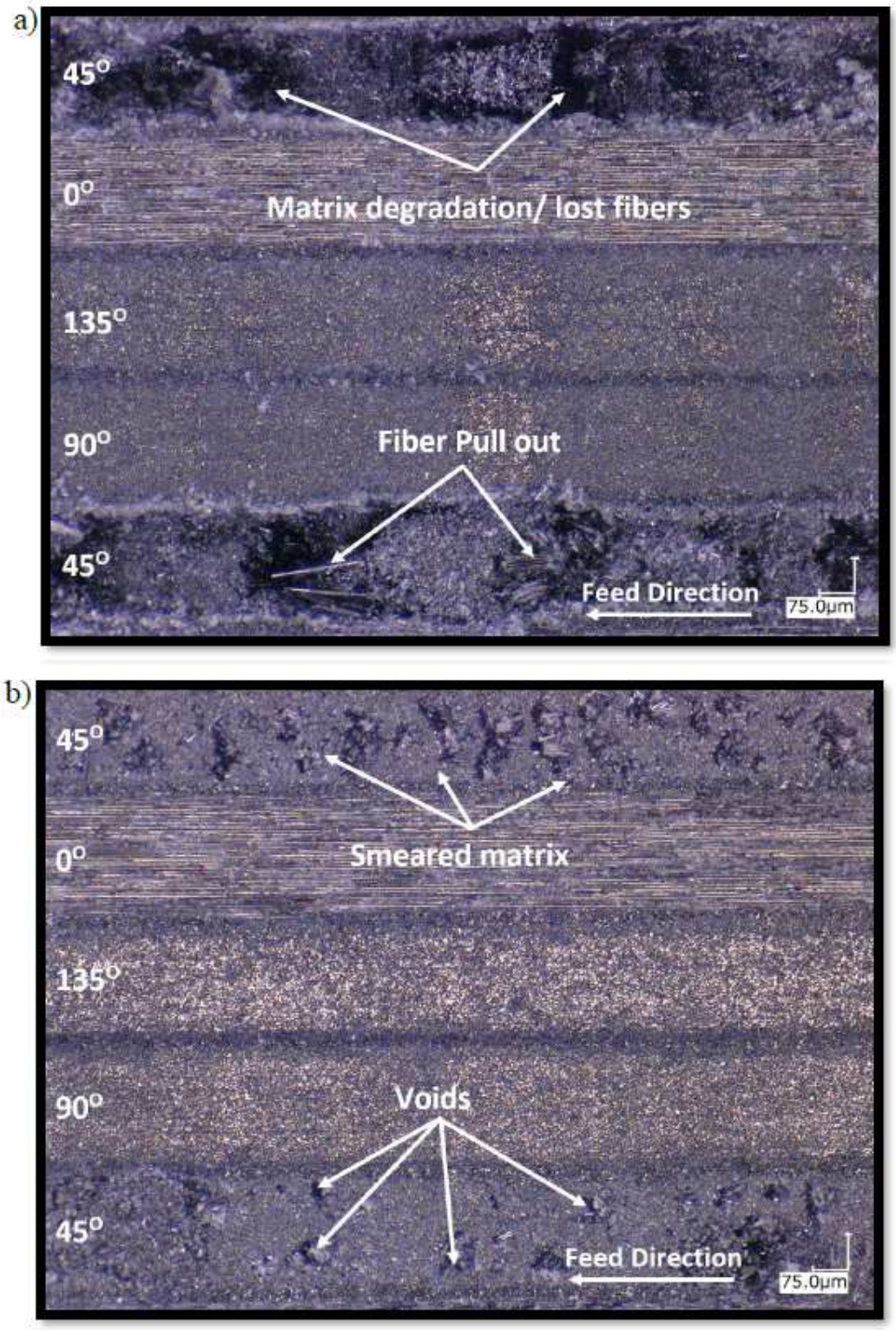

Figure 15

Effect of rake angle on surface quality at conditions of 10,000 rpm, 50 mm/min, 4.5 µm a) rake angle 0o (Test 17) b) rake angle 15o (Test 52)

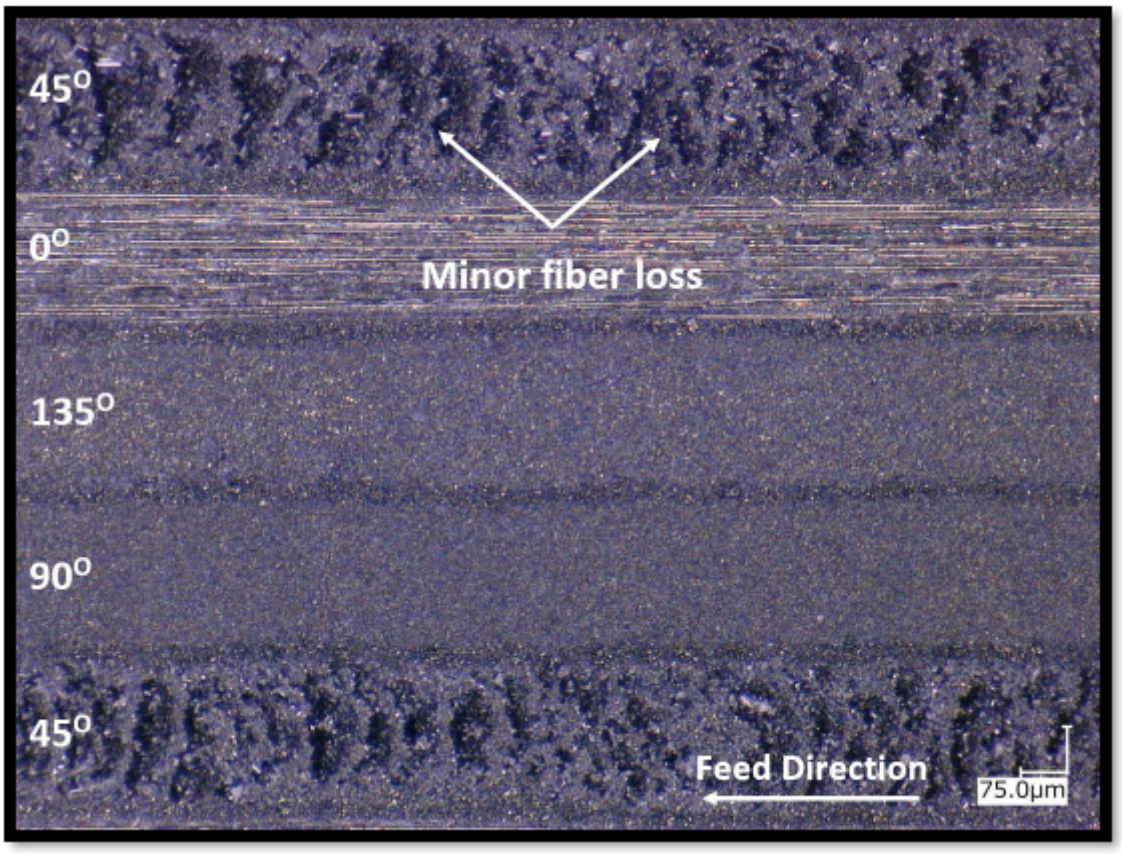

Figure 16

Effect of low spindle speed on surface quality at conditions of 5,000 rpm, 50 mm/min, 4.5 µm, and rake angle 15o (Test 26)

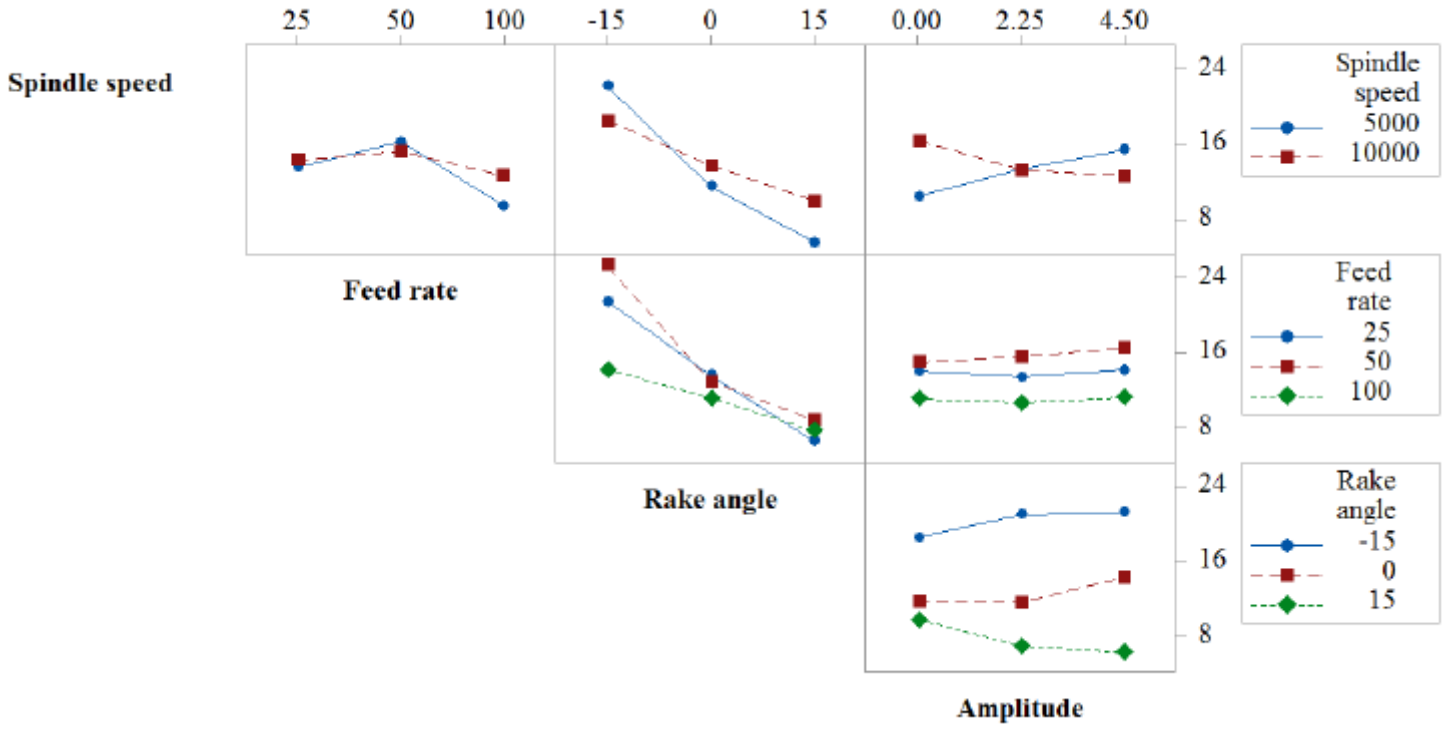

Figure 17

Interaction plot for Ra at tool engagement

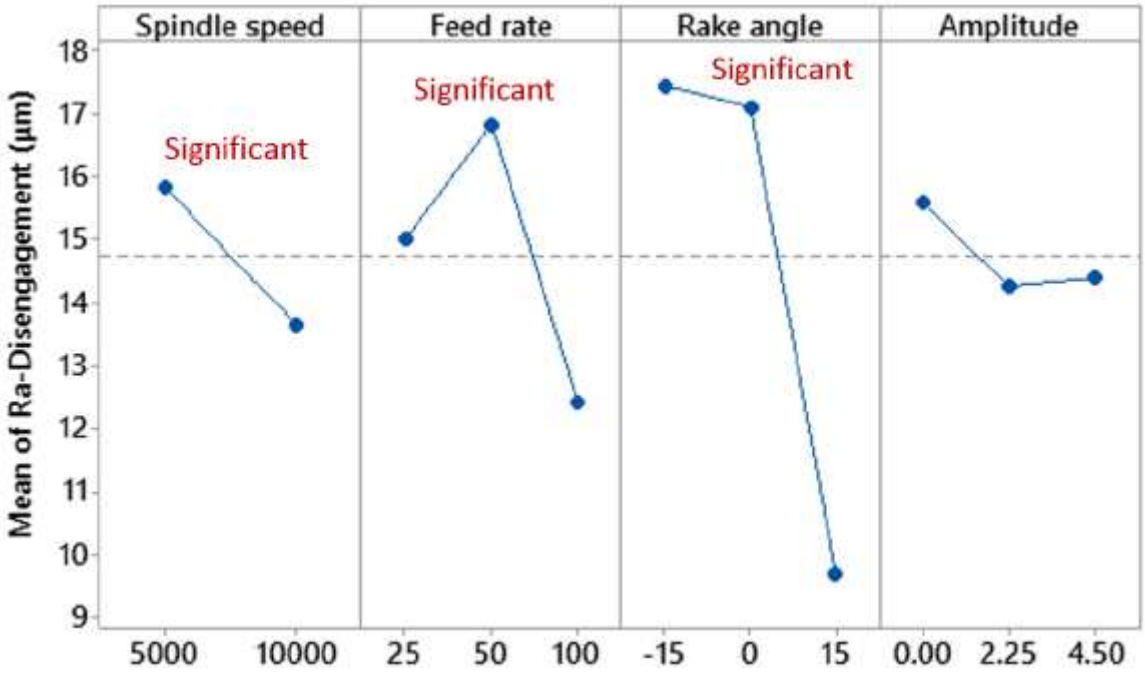

Figure 18

Main effects plot for surface roughness at tool disengagement

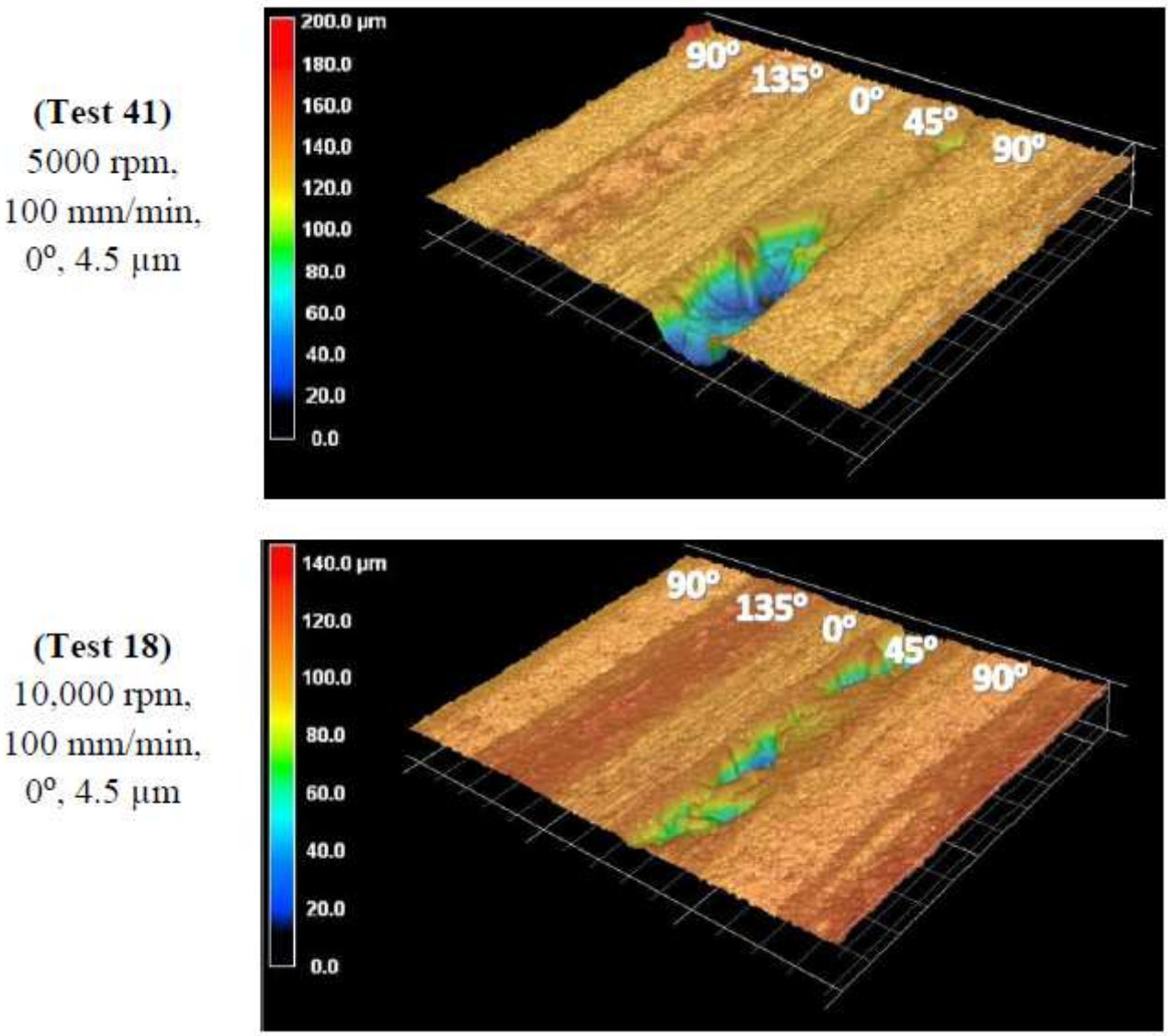

Figure 19

Effect of different spindle speed at tool disengagement

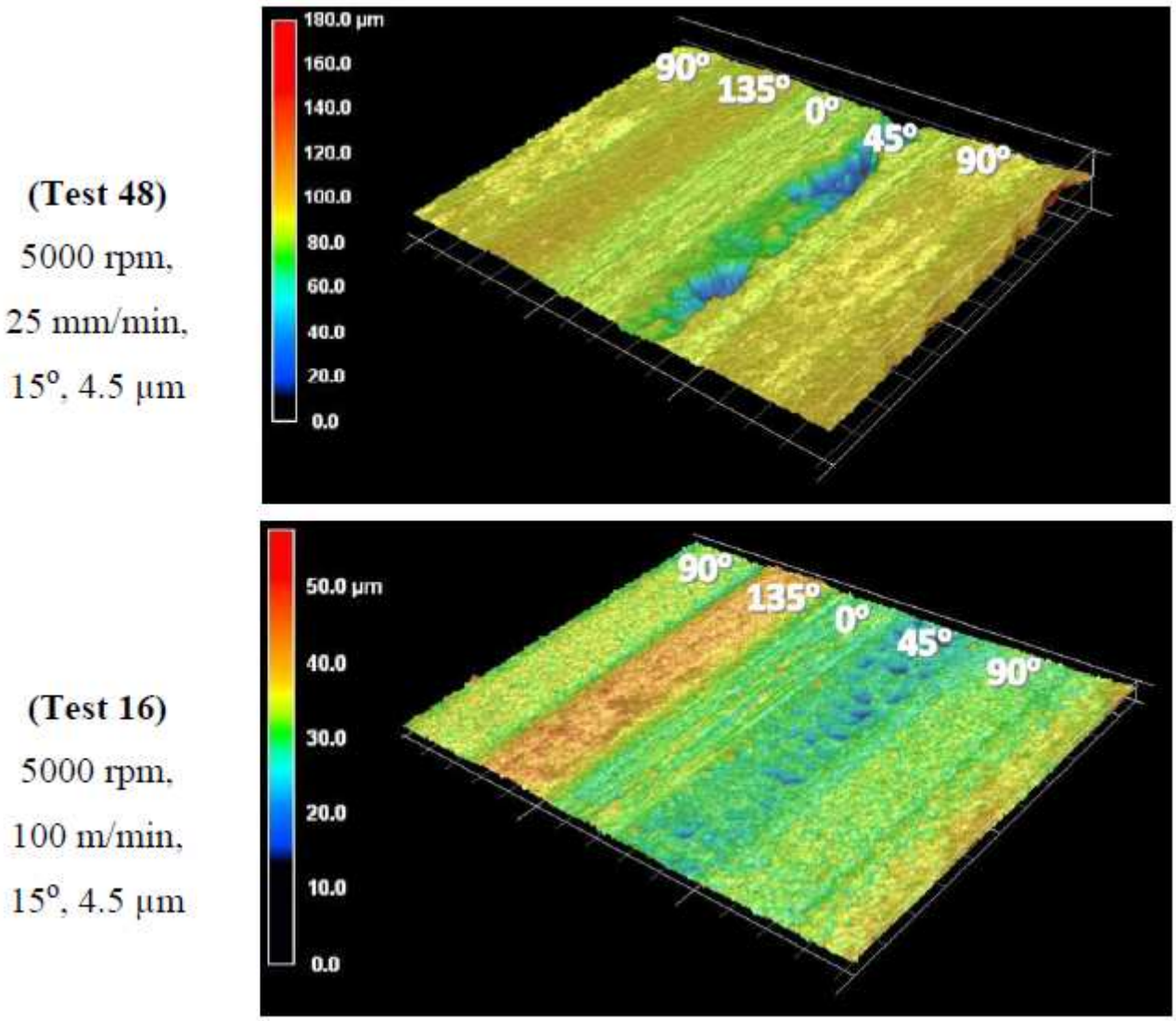

Figure 20

Effect of different feed rate at tool disengagement

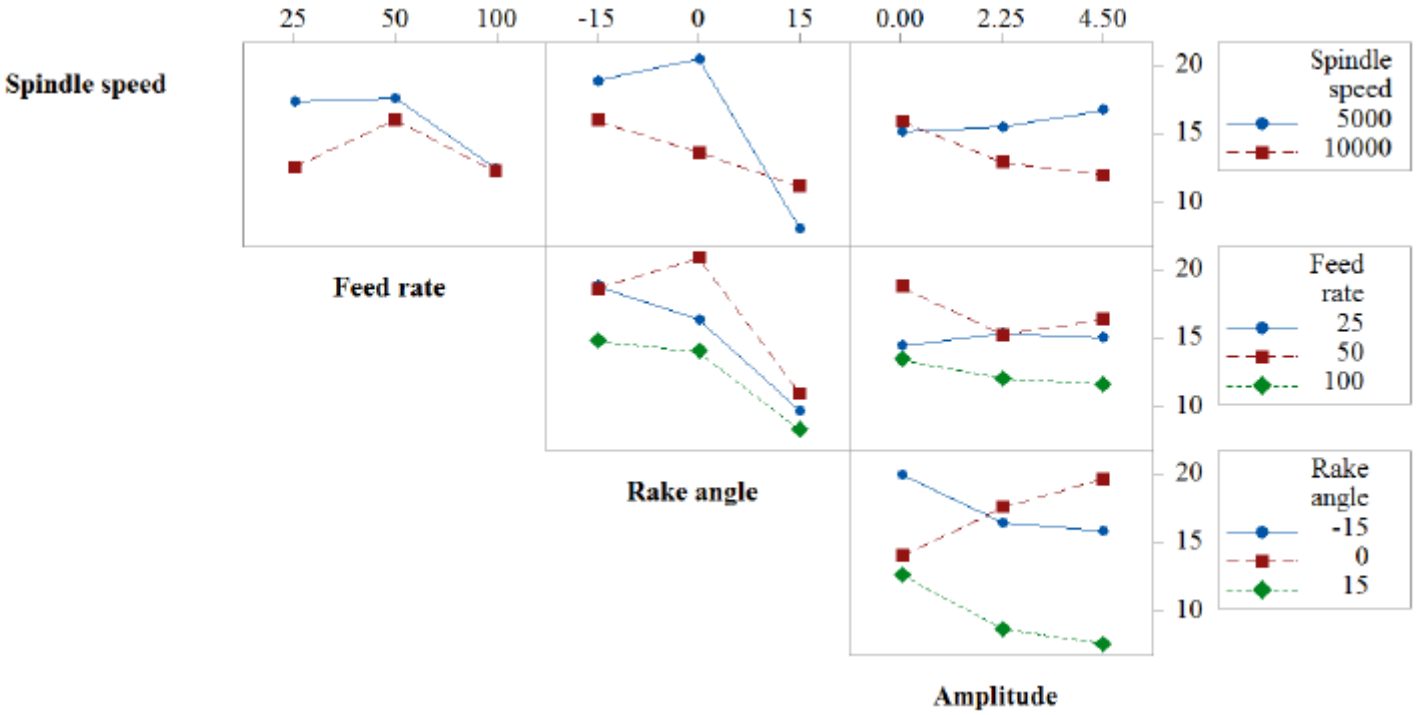

Figure 21

Interaction Plot for the Ra at tool disengagement

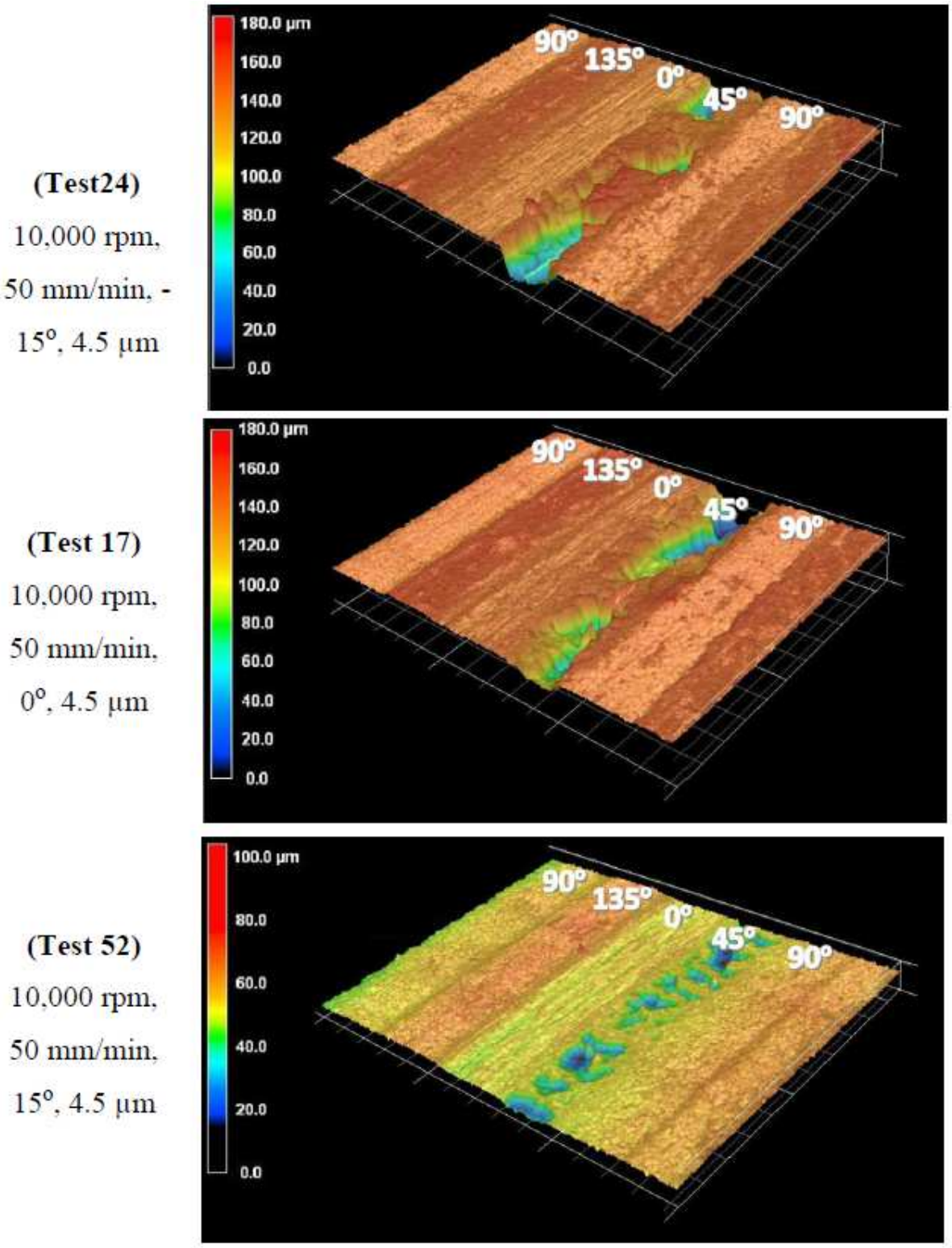

Figure 22

The 3D image of the machined surface using different rake angles at ultrasonic mode

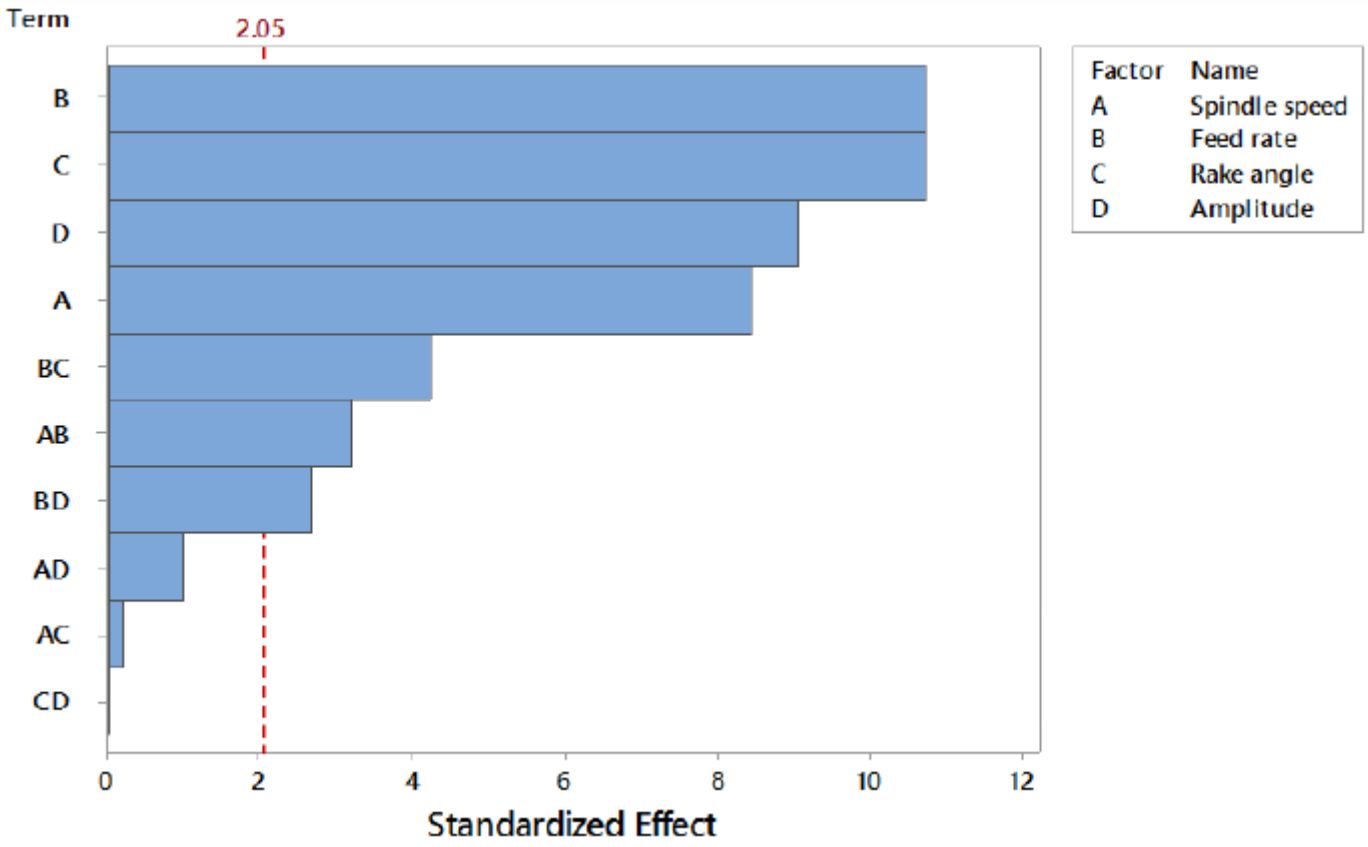

Figure 23

Pareto chart of the standardized effects on tool wear

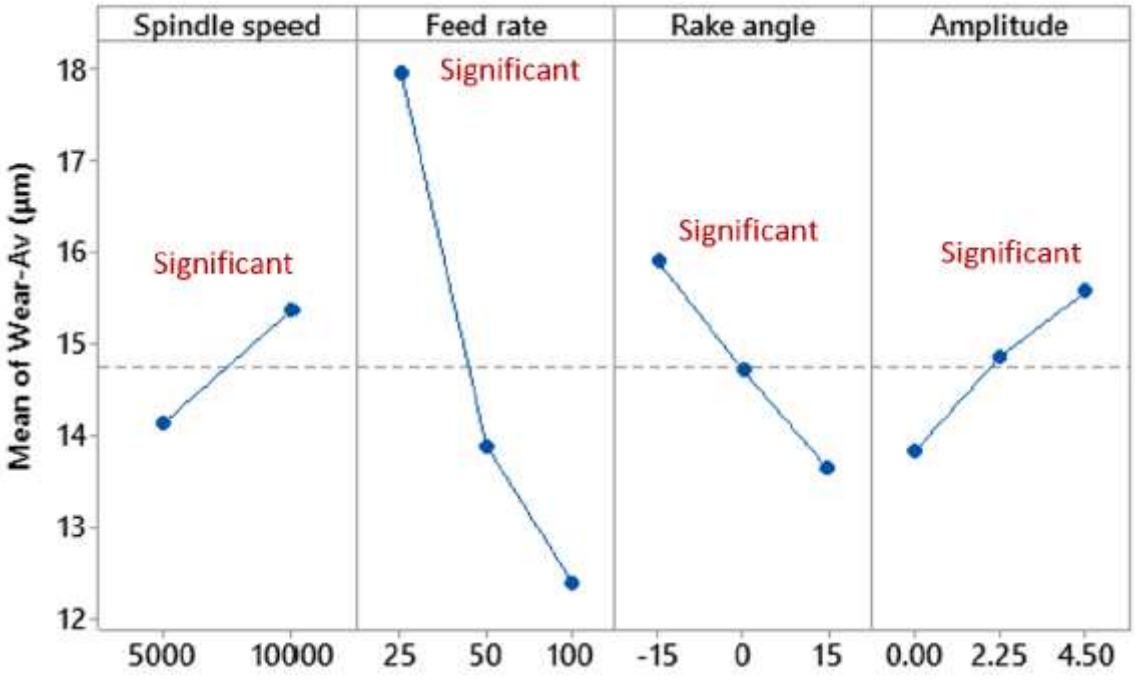

Figure 24

Main effects plot for average tool wear

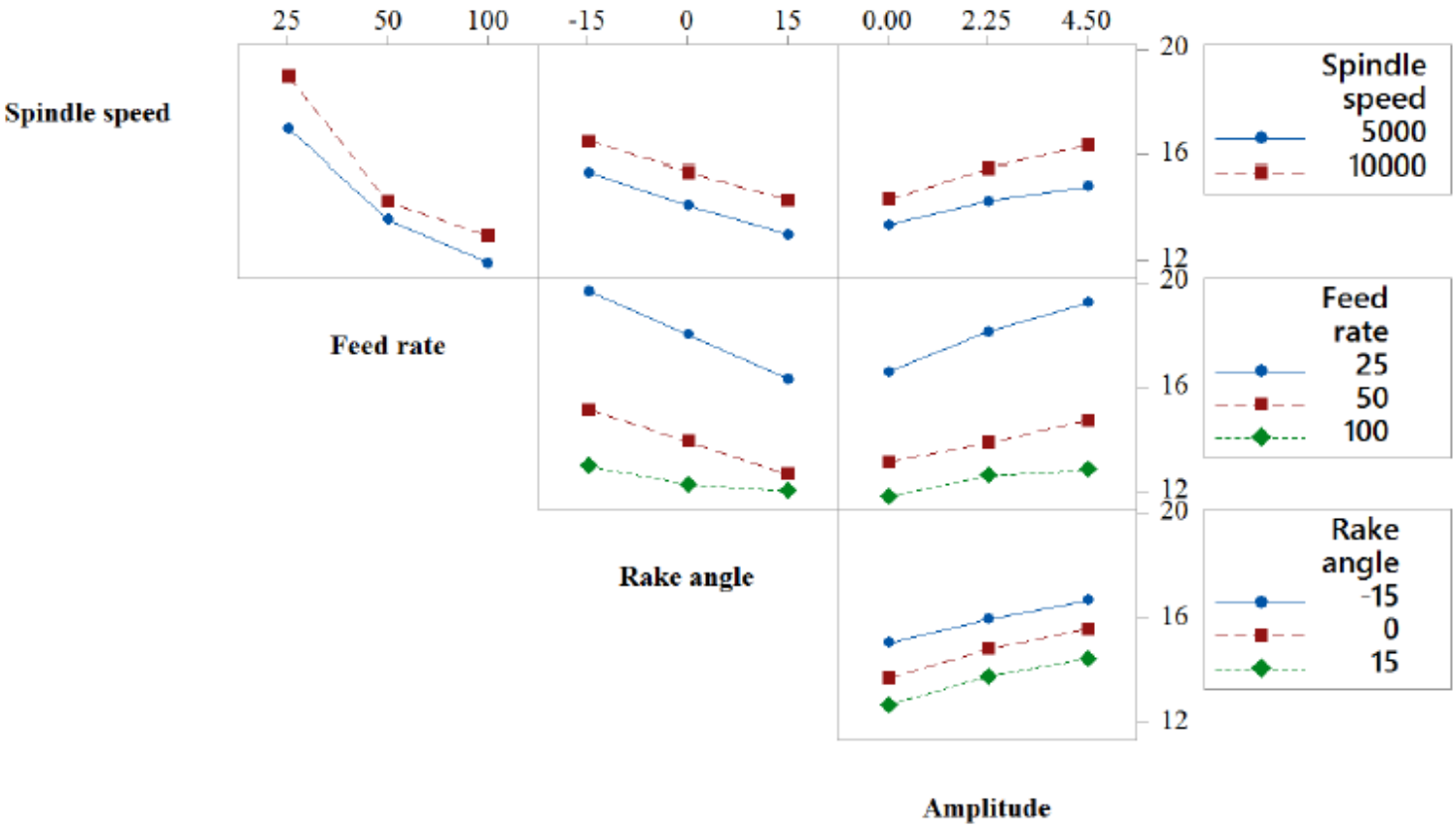

Figure 25

Interaction Plot for the Ra at tool disengagement